Studies on the Effect of Rain, Fog, and Smog on Outdoor Optical Wireless Links

A Thesis Submitted
in Partial Fulfillment of the Requirements
for the Degree of
Master of Technology

by

MANISHA AGRAWAL

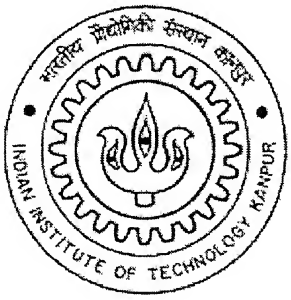

to the

Department of Electrical Engineering,
Indian Institute of Technology Kanpur

May, 2005

CERTIFICATE

This is to certify that the work contained in the thesis entitled "**Studies on the Effect of Rain, Fog, and Smog on Outdoor Optical Wireless Links**", by **Manisha Agrawal (Roll No. Y3104051)**, has been carried out under my supervision and this work has not been submitted elsewhere for a degree.

May, 2005

Dr. Joseph John,
Professor,
Department of Electrical Engineering,
Indian Institute of Technology Kanpur,
Kanpur – 208 016.

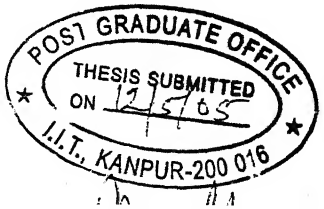

ABSTRACT

An optical wireless system is an alternate wireless system for high speed data transfer to combat the highly congested RF spectrum. Outdoor optical wireless systems are becoming more popular and gaining market acceptance as a functional wireless tool, because of their advantages such as, unlimited and unregulated spectrum, low cost etc. One barrier which still exists in the wide acceptance of optical wireless communication (OWC) Systems is the effect of the atmospheric conditions viz. rain, fog, haze, smog etc.

The main emphasis in this work is on the degradations induced by the atmosphere on the received optical signal. A comprehensive study of the existing outdoor optical links is done and their major features are compared. The major design challenges faced by an Outdoor wireless link are also discussed. The major atmospheric degradations considered are: attenuation due to fog, attenuation due to rain, and attenuation due to smog. Theoretical models for rain, fog and smog are studied in detail. These atmospheric conditions are simulated and their attenuation characteristics studied. Effect of various parameters like wavelength, particle size, distance, and particle size distributions on attenuation is also studied. Electromagnetic wave scattering patterns based on the particle size and the size parameter are simulated. A simulation package has been developed which can calculate the attenuation for a given link under the specified weather conditions. We find that the most severe atmospheric conditions are the heavy fog and smoke. Heavy rainfall conditions also cause severe losses.

Dedicated

to

My Parents

ACKNOWLEDGEMENT

A journey is easier when you travel together. Interdependence is certainly more valuable than independence. This thesis is the result of one year of work whereby I have been accompanied and supported by many people. It is a pleasant aspect that I have now the opportunity to express my gratitude for all of them.

First, I would like to thank Prof. Joseph John for his invaluable guidance throughout the thesis. His enthusiasm and integral view on research, has made a deep impression on me. I was particularly impressed by the fashion in which he explained many intricate concepts and provided a motivating, enthusiastic, and critical atmosphere during the many discussions we had.

I would like to thank Mr. A. Sivabalan, for our many discussions and providing me advises and tips that helped me a lot in staying at the right track.

I am grateful to my colleagues and friends, Smitha, Indrani, Bhaumik, Sagnik and Vinay for their excellent company and support throughout the thesis period. I would also like to thank all my classmates whose company made my stay at IIT Kanpur a memorable experience.

Last but not the least, I feel a deep sense of gratitude for my parents who formed part of my vision and taught me the good things that really matter in life

The chain of my gratitude would be definitely incomplete if I would forget to thank the first cause of this chain, using Aristotle's words, The Prime Mover. My deepest and sincere gratitude for inspiring and guiding this humble being.

Manisha Agrawal

CONTENTS

CHAPTER 4

CHAPTER 5

LIST OF FIGURES

CHAPTER 4

CHAPTER 5

LIST OF FIGURES

LIST OF TABLES

LIST OF SYMBOLS

a_n	Mie coefficient
b_n	Mie Coefficient
b_{ap}	Absorption coefficient of black carbon
b_{Coarse}	Scattering coefficient of suspended particles
b_{NO3}	Scattering coefficient of ammonium nitrite
b_{SO4}	Scattering coefficient of ammonium sulphate
c	Concentration of the scattering or absorbing species
$C(l)$	Contrast as a function of distance
C_{abs}	Single particle absorption cross-section
C_{ext}	Single particle extinction cross-section
C_{scat}	Single particle scattering cross-section
D	Diameter of the particle
D_m	Median diameter
E^i_l	Parallel component of incident electric field
E^i_r	Perpendicular component of the incident electric field
E^s_l	Parallel component of scattered electric field
E^s_r	Perpendicular component of the scattered electric field
G	Area of cross-section
h_n	Hankel function
$I(l)$	Intensity of the transmitted wave as a function of distance
I_{scat}	Intensity of the scattered wave
j_n	Bessel function of the first kind
k	Imaginary part of the refractive index
k_{ext}	Mass extinction coefficient
l	Distance between transmitter and receiver
m	Refractive index of the particle
n	Real part of the refractive index
n_n	Bessel function of the second kind
$n(r)$	Drop size distribution as a function of radius

$N(D)$	Drop size distribution as a function of diameter
Q_{abs}	Absorption efficiency
Q_{ext}	Extinction efficiency
Q_{scat}	Scattering efficiency
P_{abs}	Absorbed power
$P(l)$	Power of the transmitted wave as a function of distance
P_n	Legendre Polynomial
P_{scat}	Scattered power
$Pr(h)$	Pressure as a function of height
r	Radius of the particle
r_c	Mode radius of the particle
R	Rain rate
S_1	Scattering amplitude function
S_2	Scattering amplitude function
$T(h)$	Atmospheric temperature as a function of height
x	Size parameter
V	Visibility
α_{ray}	Rayleigh Scattering Coefficient
β_{ext}	Extinction coefficient
ε	Dielectric constant of the particle
λ	Wavelength of light
π_n	Mie angular coefficient
ρ	Density of the attenuating medium
σ	Extinction cross-section
τ	Optical thickness
τ_n	Mie angular coefficient
ψ	Ricatti-Bessel function
ζ	Ricatti-Bessel function
$\acute{\Gamma}$	Gamma Function

CHAPTER 1
INTRODUCTION

Over the last decade, there has been a steady increase in the number of consumers using high capacity data transmissions, and their data rate demands have risen from hundreds of megabytes per second to tens of gigabytes per second. There is little room left in the radio frequency spectrum to add more transmitting channel. For this reason, many companies turned up towards the light as a way to provide the needed room for communication expansion. Also, advancement in optical devices has led to an increasing number of applications for optical communication systems. These systems consist of both guided and unguided communication links, termed Optical Wireless Communication (OWC) Links.

In contrast to guided systems such as the fiber optic cables used in telephone networks, unguided systems launch light into a medium without any attempt to control the propagation of the light after it leaves the transmitting optics. Unguided systems offer numerous advantages over RF systems including higher data rates and less side lobe interference. Also, the narrow beam allows for higher antenna gain and smaller antennas. The improvement in system performance over RF designs can be used to decrease power, size and weight requirements, an important consideration for satellite payloads which are constrained by these parameters. The disadvantages of unguided optical systems include the requirement of accurate beam pointing and the degradations inflicted by the medium of propagation, such as air or water. Figure 1.1 is an example of an OWC system.

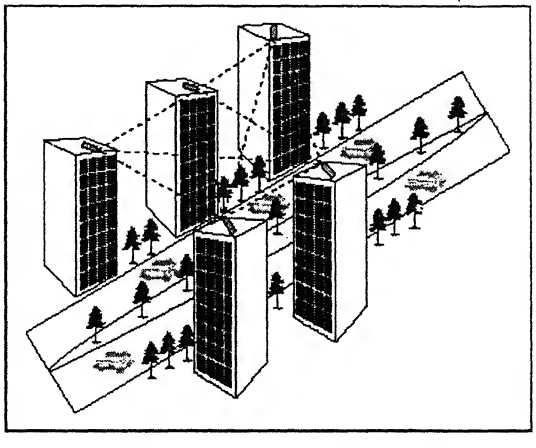

Figure 1.1. Example of Optical Wireless Network [1]

The emphasis in this thesis is on the degradations induced by the atmosphere on the received optical signal. The major degradations included in this study are: 1) Attenuation due to fog, 2) Attenuation due to rain, 3) Attenuation due to smog. Since outdoor optical hardware and prototypes are expensive and inflexible, simulation is an attractive alternative for predicting the performance of optical systems. Well established simulation models exist for the guided medium, but for unguided systems an end-to-end simulation is very much required. It is the objective of this thesis to simulate the various degradations introduced by the atmosphere on the performance of outdoor optical wireless links.

Advantages of OWC systems

a) Easy to deploy,
b) no tariffs are required for its utilization (an operating cost saving),
c) there are no RF radiation hazard (when eye safe power levels are maintained),
d) has large bandwidth, which facilitates high data rates,
e) very compact transmitting and receiving modules, possible for short range applications,
f) has low power consumption,
g) exploits unused part of the electromagnetic spectrum,

Disadvantages of OWC systems

a) requires accurate pointing and alignment between transmitter and receiver,
b) dependent on atmospheric effects – rain, fog, smog and snow outages,
c) less suited to broadcasting because of the narrow optical beam,
d) selectivity and availability of sources and detectors in suitable bands.

1.1 APPLICATIONS OF OPTICAL WIRELESS COMMUNICATIONS

Optical Wireless communication can bridge the gap by enabling connection with offices, business facilities, and other targeted locations without relinquishing the performance parameters offered by Radio Communication. Some of the short range, long range, and wide area applications are listed below.

Short Range Applications

- Weather monitors; fog, snow, rain using light back-scatter,
- Traffic counting and monitoring,
- Optical Interconnects.

Long Range Applications

- Deep space probe communications; distances measured in light-years,
- Building to building very high data rate computer data links;
- Ship to ship communications with high data rates and security,
- Telemetry transmitters from remote monitors for weather, geophysical, etc.
- Electronic distance measurements, such as hand held units out to 1000 ft.,
- Optical radar; shape, speed, direction and range,
- Remote telephone links, which are cost effective than microwave links.

Wide Area Applications

- Campus wide computer networks,
- City-wide information broadcasting,
- Inter-office data links.

1.2 THESIS OBJECTIVES

The main objective of the thesis is to study the effect of rain, fog, and smog on the performance of outdoor optical wireless links. This involves the following tasks.

- Review of outdoor optical links.
- Understanding the various aspects of outdoor optical communication systems under different atmospheric conditions.
- Theoretical study of the drop size distributions under different atmospheric conditions.
- Simulation of various atmospheric losses with different link design parameters.
- Graphical representation of all the losses studied.
- Developing a simulation package to calculate the atmospheric losses for the given atmospheric condition.

1.3 THESIS ORGANIZATION

Chapter 2 gives a review of the outdoor optical links. A brief comparison of the presently available systems are also discussed.

Chapter 3 deals with the various design issues and challenges, such as selection of wavelength, scattering, absorption, etc., encountered in an outdoor optical wireless link.

Chapter 4 is devoted to the theoretical study of the effect of various atmospheric conditions on outdoor optical wireless links, i.e., the effect of rain, fog , and smog.

Chapter 5 gives the simulation methodologies of outdoor wireless links. The effect of the rain, fog and smog on the outdoor optical links is simulated and plotted. An analysis on those results is also presented.

Chapter 6 concludes the thesis with the major results and gives suggestions for further work in this area.

CHAPTER 2
REVIEW OF OUTDOOR OPTICAL WIRELESS LINKS

2.1 INTRODUCTION

Outdoor optical wireless communication (OWC) systems use light to communicate through the air, and require line of sight between the transmitter (Tx) and the receiver (Rx) units. Modern systems typically use lasers at the transmitter to transmit the signal and photo diodes at the receiver to detect the incoming light and send an appropriate signal for processing. Outdoor OWC systems may be used for medium to very high data ratc applications. Increasingly these systems are used for high-bandwidth applications needing data transfer of hundreds of megabits per second. Moderately priced OWC consumer products are now available.

2.2 A BASIC OUTDOOR OPTICAL LINK

There are three key functional elements of a free space OWC system, viz. the transmitter, the atmospheric channel, and the receiver. The transmitter converts the electronic signal into light. The light propagates through the atmosphere to the receiver, which converts the light back into an electronic signal. The transmitter includes a modulator, a laser driver, a LED or laser, and a collimator. The modulator converts bits of information into light signal in accordance with the chosen modulation method. The driver provides the power for the laser and stabilizes its performance; it also neutralizes such effects as temperature and aging of the laser or LED. The laser is characterized by its central wavelength, average power, and beam divergence angle. Ideally, its frequency spectrum is sufficiently narrow to allow optical analysis to relate to the central wavelength alone. The LED is a lower power source. It is often preferred to the laser as a cheaper alternative, and is becoming increasingly attractive with the recent developments in super-luminescent LEDs with relatively narrow bandwidths and up to 70 mW power outputs. The beam divergence angle determines the free space power loss, or how large the laser spot will be at a given distance from the source. The collimator aligns the laser-LED radiation to a collimated beam and directs it to the receiver.

The receiver includes a telescope, a filter, a photo-detector, an amplifier, a decision device and a clock recovery unit. The telescope collects the incoming radiation and focuses it onto the filter. The filter removes background radiation and allows only the wavelengths of the signals to pass through it. The photo-detector converts the optic radiation into an electronic signal, and the amplifier amplifies the electronic signal. The decision unit determines the nature of the bits of information based on the time of arrival and the amplitude of the pulse. The clock recovery unit operates in parallel to the decision making unit and synchronizes the sampled data into the decision making process. The quality of reception is measured by the probability of error, expressed in terms of the bit error rate (BER).

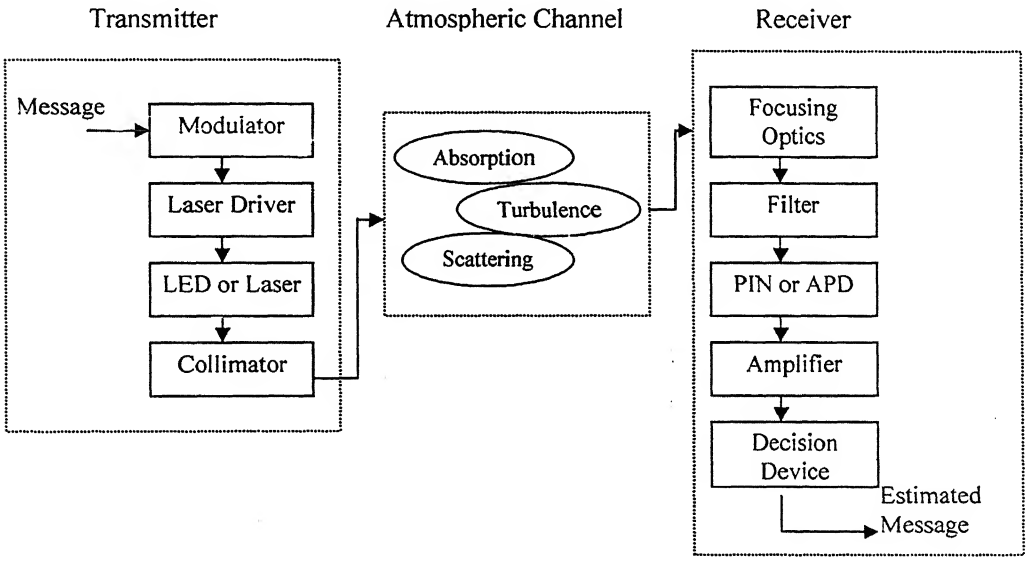

Figure 2.1 Block diagram of Optical Wireless Communication Link

The transmitter and the receiver are separated by the propagation channel, which is the atmosphere in the case of OWC. Even on an apparently clear day the atmosphere is pervaded by molecules and aerosols, which cause absorption and scattering of the light. Changes in the temperature along the propagation path lead to scintillations in the received light due to resultant turbulence.

Line of sight is imperative for outdoor OWC systems, and may be maintained with the help of a tracking and pointing system. Tracking is performed in two stages,

coarse tracking and fine tracking. Coarse tracking may use GPS or other a priori knowledge. Fine pointing requires electro-optic mechanisms such as a quadrature or matrix detector. Pointing involves a beam-steering device which may be mechanical, such as a galvo-mirror, or non-mechanical, such as acousto-optic crystals, electro-optic devices or optical phased arrays.

2.3 LITERATURE REVIEW

Free-space optical communication has attracted considerable attention recently for a variety of applications. Gagliardi [2] has studied outdoor optical communication systems in good detail. Analysis and design of an OWC system is discussed in detail. A review of optical fields, sources, channels and signal descriptions is also presented.

The effects of wind, earthquakes, and thermal expansion on an OWC system are described by Kim *et al.* [3]. They studied the transmission of high speed computer network data on the free space channel and also discussed a tracking system to nullify the effects of building sway to maintain alignment between the transmitter and the receiver.

Leeb [4] gives the background radiation effects on the transmission of optical signal through the atmosphere and studies the degradation of the signal to noise ratio with the background illumination.

Studies based on available weather statistic measurements indicate that the weather effects can be mitigated by use of medium- and far-IR laser sources. Chapasso *et al.* [5] discuss the quantum cascade lasers (QCLs), which are adjusted to operate within the atmospheric window regions in the mid-wave and long-wave IR wavelengths. They demonstrated the use of QC Lasers in effectively mitigating the various atmospheric effects.

A comprehensive study of the effect of turbulence on communication links is described by Brookner [6]. Davis [7] studied the signal to noise ratio for an AM signal passing through the turbulent atmosphere and also the probability of detection of fluctuating laser signals.

The effect of fog on the bit-error rate of a free-space laser communication system is discussed by Strickland *et al.* [8]. The paper shows that the BER increases as the optical depth (which is defined as the extinction coefficient over the length of the channel) increases which in turn leads to increase in the atmospheric attenuation.

Grotzinger [9] discussed about the performance of free space systems under different weather conditions. He also discussed fade margin and gave a review of the methods that can be employed to improve the fade margin.

Kim *et al.* [10] studied suitable wavelengths for the propagation of laser beam in foggy conditions. They showed that in dense fog (i.e. for visibility < 200 m) the attenuation of the laser beam is independent of wavelength and all are equally attenuated by fog. For light and moderate fog conditions (i.e. visibility < 500 m) 1550 nm wavelength is less attenuated than the 785 nm wavelength. They formulated a new equation for the atmospheric attenuation under different visibility conditions.

Acampora *et al.* [11] proposed a hybrid access network that uses small radio cells, where the cell base stations are interconnected by optical wireless links. As the links are for a short ranges (typically a tens of meters), the system is almost immune to all the extreme weather related impairments.

Achour [12] presented a review of the effects of rainfall on free space optical signal propagation. He presented a simulation model for the computation of atmospheric attenuation with respect to the rainfall rate.

Achour [13] presented a review on the effects of fog, haze and low clouds on free space optical signal propagation. He presented a simulation model for the computation of atmospheric attenuation under the above conditions.

Satle [14] studied the performance of the outdoor short range (up to 30m) optical wireless links under clear weather and fog conditions. He conducted a few experiments in fog conditions and established a relationship for the atmospheric loss.

2.4 OUTDOOR OPTICAL COMMUNICATION SYSTEMS (PRESENT STATUS)

Optical communications is one of the cornerstones of today's revolution in information technology. With the drive towards portable and multimedia communications, we are increasingly faced with the challenge of bringing the capacity of our communication infrastructure directly to the user, providing seamless access to huge quantities of information, anywhere and anytime. Whether it is the transfer of an image from a digital camera to a laptop computer or the communication of data within a massively parallel computer, there is an urgent need to develop new methods of high speed data communications. Light offers many advantages as a medium for communication. Whether traveling through free space or through optical fiber, light provides large channel bandwidth and data rates in the range of terabits per second. This immense capacity is due to the nature of the photons that constitute an optical signal. Unlike electrons, photons react weakly to their environment and to one another. As such, optical signals neither generate nor are sensitive to electromagnetic interference (EMI), parasitic coupling, and other problems faced by the electrical signals. Due to their advantages, optical wireless links are becoming more popular in application areas as compared to traditional Radio and fiber-optics. Some of the major companies and their outdoor Optical Wireless Systems are listed below.

- Dominion Lasercom Inc. [15] –

Product Name	Link Distance	Data-rate	Wave-length	Type of Transmitter	Output Power	Type of Detector
Skyfiber	2 km	100 Mbps	780, 808, 850nm	AlGaAs Multimode	30-100mW	-
Skyfiber	2 km	10 Mbps	780, 808, 850nm	AlGaAs Multimode	30-100mW	

- Laser Wireless Systems [16]

Product Name	Link Distance	Data-rate	Wavelength	Type of Transmitter	Output Power	Type of Detector
ExoLACE E155	3 km	155 Mbps	810 nm	AlGaAs Laser Diode	25 mW	Si APD

- Light Pointe Systems [17]

Product Name	Link Distance	Data-rate	Wavelength	Type of Transmitter	Output Power	
FlightApex	1.3 km	2.5 Gbps	1550 nm	EDFA	-	InGaAs APD
Flightstrata						
FSA52E, FSA52EW	5.6 – 5.2 km	1.5 Mbps to 54 Mbps	850 nm	VCSEL	-	Si APD
FSA155E, FSA155EW	4.8 – 4.4 km	1.5 Mbps to 155 Mbps				
FSA622	3.3 km	622 Mbps				
FSA-G	2.0 km	1.25 Gbps				

- Cable Free Solutions Inc. [18]

Product Name	Link Distance	Data-rate	Wavelength	Type of Transmitter	Output Power	Type of Detector
CF Access A31000	3 km	155 Mbps	980 nm	-	-	Enhanced APD
CF 622 Series CF 2000	2 km	622 Mbps	780 nm	-	-	APD
CF Gigabit G 1000	1 km	1.5 Gbps	780 nm	-	-	APD

- Plain Tree Systems [19]

Product Name	Link Distance	Data-rate	Wavelength	Type of Transmitter	Output Power	Type of Detector
WB500	1 km – 2 km	10 – 100 Mbps	800 – 900 nm	LED		-
WB600	500 m	155 Mbps	800 – 900 nm	LED		-

- MRV Communications Inc. [20]

Product Name	Link Distance	Data-rate	Wavelength	Type of Transmitter	Output Power	Type of Detector
Terescope 155 Series						
TS 3101	520 m	155 Mbps	850 nm	1 LED	1.1mW	Si PIN
TS 3303	1.7 km			3 VCSEL	19.5 mW	
TS 4900	4.2 km			4 VCSEL	100 mW	
Terescope 34 Series						
TS 802/ST	1.2 km	34 Mbps	850 nm	1 LED	0.8 mW	Si PIN
TS 811/ST	3 km			3 VCSEL	19.5 mW	
TS 940/ST	4 km			4 VCSEL	24 mW	
Terescope 10 Series						
TS707/ETH	2 km	10 Mbps	850 nm	3 LED	8 mW	Si PIN
TS980/ETH	5.9 km			4 VCSEL	100 mW	
Terescope 2 Series						
TS702/E1 TS702/T1	1 km	E1 – 2.048 Mbps T1 – 1.55 Mbps	850 nm	1 VCSEL	0.8 mW	Si PIN
TS811/E1 TS811/T1	2.9 km			3 VCSEL	19.5 mW	
TS960/E1 TS960/T1	6 km			4 VCSEL	32 mW	

- Fsona Systems Corporation [21]

Product Name	Link Distance	Data-rate	Wavelength	Type of Transmitter	Output Power	Type of Detector
8 –E	50 m – 4.95 km	1.5 – 10.5 Mbps	1550 nm	Laser Diode	100 mW	-
155 E	20 m – 2.6 km	1.5 –160 Mbps				
155 –E	100 m – 3.8 km	31 – 180 Mbps			320 mW	
1250 E	100 m – 3.2 km	100 - 1448 Mbps			280 mW	
2 M	300 m – 7.7 km	31 – 62 Mbps			640 mW	
1550 M	400 m – 5.3 km	100 – 1448 Mbps			560 mW	

- Laserbit Wireless Cables [22]

Product Name	Link Distance	Data-rate	Wavelength	Type of Transmitter	Output Power	Type of Detector
LB 1500	1.5 km	155 Mbps	785 nm	Laser Diode	2 x 70 mW	APD
LB 2500	2.5 km				4 x 70 mW	
LB 5000	5 km				8 x 70 mW	

The commercially available links are broadly divided into two categories. Short range links (having link range less than 2 km) and long range links (having link range greater than 2 km).

Short Range Links

Light Pointe Communications Inc. has introduced two short range products FlightApex and FlightStrata for up to 1.3 km and 2 km link range and 2.5 and 1.25

Gbps data rates, respectively. Cablefree Solutions Inc. has also launched a product range CF Gigabit, having a link range of 1 km operating at a data rate of 1.5 Gbps. Canonbeam from Canon and CF 622 product range from Cable free Solutions Inc. is available for link ranges up to 2 km at 622 Mbps. For the speed of 155 Mbps, many companies viz. Cablefree Solutions, Fsona Systems Corporation, Laserbit Wireless Cables and Dominion Inc. have a wireless link up to a distance of 2 km. While most products are only for point to point communications, companies such as AirFiber and Terabeam have brought out products that easily allow a mesh of links to be set up.

Long Range Links

There are a number of long range products available for the different data rates for link ranges up to 7 km. Fsona System Corporation's M and S Series range of products provide links from 3.3 km to 7.7 km range for data rates starting from 31 Mbps to 1.448 Gbps. For the link range of 3.5 km, LightPointe Communications Inc. provide data rate of 622 Mbps. For the speed of 155 Mbps and lower, many companies viz. Cablefree Solutions, Fsona Systems Corporation, Laserbit Wireless Cables and Dominion Inc. have wireless links up to a distance of 5km. The power level employed for the long distance links generally fall into class 3 eye-safe. LSA Photonics has introduced a product for relatively lower data rate (45 Mbps) but longer ranges (up to 15 km).

In this chapter a brief review of all the advancements that has taken place in this field is given. A comprehensive review of all the existing outdoor links has also been presented and compared. In the next chapter, the design challenges that are faced by the OWC system are discussed.

CHAPTER 3
DESIGN CHALLENGES IN OUTDOOR OPTICAL WIRELESS LINKS

With the optical wireless communication becoming very popular, there is a need to build robust optical transmitters and receivers for establishing point to point communication through the atmosphere. Despite the advantages, there are some important design issues associated with the OWC systems. Some of the major design challenges faced by an OWC system are selection of wavelength, selection of source and detector, problem of alignment between transmitter and receiver, atmospheric effects such as absorption, scattering and turbulence. These issues are briefly discussed in the following section.

3.1 SELECTION OF WAVELENGTH

Performance of OWC systems depends a lot on the wavelength used for communication, thus making the selection of wavelength a crucial issue. The two factors which needs consideration while specifying the operating wavelength are the eye safety issue and the atmospheric attenuation.

The system must not pose any danger to the people who encounter the beam. Therefore a laser safety standard has been established in which optical sources have been classified in accordance with their total emitted power. The principal classifications are summarized in Table 2.1 for a point source emitter such as the semiconductor laser [23].

Outdoor point-to-point systems generally use high power lasers that operate in the class 3B band to achieve a good power budget. The 780 to 850nm wavelength band is presently the best choice for most applications of optical wireless links, due to the availability of low cost laser diodes (LDs). It also coincides with the peak responsivity of inexpensive, low capacitance silicon photodiodes. The primary drawback of radiation in this band relates to the eye safety; as the radiation at this band can pass through the human cornea and be focused by the lens on to the retina, causing thermal damage. The cornea is opaque to radiations beyond 1400nm,

considerably reducing potential ocular hazards, so that it has been suggested that the 1550 nm band may be better suited for infrared links. It may be noted that the allowable safe power at 1550nm is about 50 times higher than that at 800nm [1].

Wavelength	650nm	880nm	1310nm	1550nm
Class1	Up to 0.2mW	Up to 0.5mW	Up to 8.8mW	Up to 10mW
Class2	0.2-1mW	N/A	N/A	*N/A*
Class3A	1-5mW	0.5-2.5mW	8.8-45mW	10-50mW
Class3B	5-500mW	2.5-500mW	45-500mW	50-500mW

Table 3.1 Laser safety classifications for a point source emitter

Second issue is the atmospheric attenuation. Atmospheric optical attenuation processes are wavelength dependent, such as Rayleigh scattering from air molecules which varies as the fourth power of wavelength. The other attenuation process is Mie-scattering which causes more attenuation than Rayleigh scattering. The wavelength dependence of Mie scattering is sensitive to the nature of fog droplets; stronger when the size of the droplet is nearly equal to the wavelength of light. But in light fog and haze the attenuation due to Mie scattering is less. The wavelength dependence of the scattering coefficient β is given by [11].

$$\beta = \frac{3.91}{V}\left(\frac{\lambda}{550nm}\right)^{-q} \tag{3.1}$$

where V is visibility in km, and $q = 0.585\,V^{1/3}$, for V<6 km. Hence for OWC links used in high fog situations, lower wavelength source will be the right choice.

Another factor affecting the wavelength selection is the beam spreading due to diffraction which is linearly proportional to the wavelength [23]. The resulting attenuation can be given by $(4\pi\, A_t / \lambda^2)$ where A_t is the transmitting area.

For terrestrial OWC links the other challenging issue is the background radiation due to sunlight [23]. The solar background radiation is four times less effective for 1550nm than for 800nm .The performance of receiver is also wavelength dependent. Generally the photodiodes near 800 nm and 1550 nm achieve comparable quantum efficiency. The output response of the detector depends on the energy of the

photon. A photon at 800nm has roughly double the energy of that at 1550 nm. Hence for the same noise conditions, the optical energy at 1550 nm will be approximately 3dB less. This necessitates higher receiver sensitivity in the case of 1550 nm systems. Also the capacitance and gain of the APD are also wavelength dependent quantities. Hence the selection of wavelength for an OWC system should consider all above factors.

3.2 SELECTION OF SOURCE

Typical lasers used in OWC are edge-emitting semiconductor devices, with wavelengths 785, 850, 980 or 1550 nm. Various output powers and wavelengths are available. Lasers have the advantages of high output powers, high modulation rates, and if cooled, long-term reliability. Nowadays, VCSELs (vertical-cavity surface-emitting lasers) are also becoming very popular as transmitting devices [18].

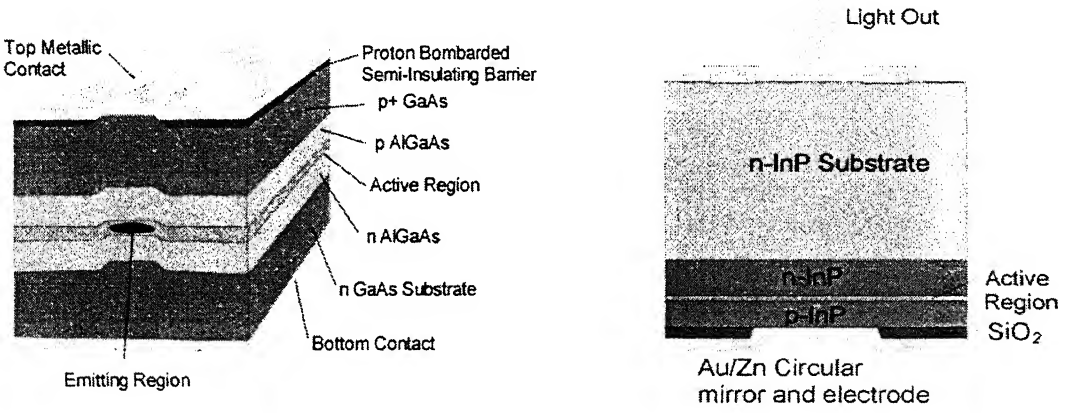

Edge Emitting Laser VCSEL

Figure 3.1 Types of sources for OWC systems

VCSELs are designed using a vertical cavity, and as a surface emitter, emits light out of its top surface. This sets VCSELs apart from all other lasers, classed as edge-emitters, which have a cavity that lies in the plane of the wafer (usually thought of as horizontal) and emits light out of the side.

VCSELs operating at 850 nanometers have become popular in Local Area Networks due to the following factors.

- At 850nm, VCSELs are cheap, and offer high bandwidths.

- VCSELs emit a uniform, narrow, circular beam, which simplifies optical system design considerably. In contrast, edge-emitters have an elliptical beam, which is strongly divergent.
- A VCSEL laser cavity is very short, compared to that of an edge-emitter. So, when the laser is turned off, it takes less time for the remaining light to exit the cavity. As a result it is possible to modulate the laser (turn the beam on and off) directly, which avoids the need for an external modulator. Devices with direct modulation speeds of 2.5 Gbps are common place.
- VCSELs are very efficient at turning injected carriers into photons. Typical efficiencies are in the region of 6 to 25 per cent. As a result they consume less electrical power than an equivalent DFB (distributed feedback) laser. For example, a DFB laser might draw 60 mA, while a VCSEL would only require 15 mA to produce the same optical output.

The problems associated with the use of VCSELs are:

- VCSELs have an abrupt failure mechanism. Long-term-reliability at moderate-to-high temperatures is a problem, and hence VCSELs have been dominant in LAN environments and not in telecoms, where high reliability is paramount.
- The materials used to make 850nm VCSELs are not yet applicable to longer wavelengths. Currently, commercial VCSELs that operate at the wavelengths of 1310 or 1550 nm have yet to become generally available.

LEDs are also used in some OWC links but only for very low cost short range systems.

3.3 SELECTION OF DETECTOR

There are a number of factors to be considered while examining the effectiveness of the receiver in an OWC system; these include the type of detector used, the sensitivity rating and size of the detector, the size and design of the receiver optics [18]. Optical detectors used in OWC equipment come in two basic types: PIN and APD. The PIN detector is a lower cost detector that has no internal gain, while the APD is a more expensive but also more sensitive detector with internal gain.

Parameter	PIN Photodiodes	APDs
Construction Materials	Si, Ge, InGaAs	Si, Ge, InGaAs
Wavelength	0.6 to 1.8 μm	0.6 to 1.8 μm
Responsivity	0.5 to 0.85 Amps/Watt	0.5 to 100 Amps/Watt
Gain	1	10 - 150
Support Circuitry Required	None	High Voltage, Temperature Stabilization
Cost	Low	High

Table 3.2 Comparison of PIN photodiode and APD

One of the key parameters to consider when selecting a detector is spectral noise. A detector normally operates in one of two noise-limited detection regimes; either detector noise limited at low power levels, or photon shot noise limited at higher power level. In an APD, sensitivity at low light levels will be limited by the shot noise and the APDs leakage current. Shot noise derives from the random statistical fluctuations of the dark current, and signal current. Dark current or shot noise in a PIN differs for an APD, as in an APD the bulk leakage current is multiplied by the gain, M, of the APD. In addition, the avalanche process statistics generate current fluctuations, and APD performance is degraded by an excess noise factor (F) compared to a PIN. At higher signal light levels, the detector transitions to the photon shot noise limited regime. In the absence of other noise sources, an APD provides a signal-to-noise ratio (SNR) which is worse than a PIN detector with the same quantum efficiency. An APD, however, can produce a better overall system signal-to-noise ratio than a PIN detector in cases where the APD internal gain boosts the signal level without dramatically affecting the overall system noise. In summary, an optical receiver using an APD offers superior sensitivity than PIN at medium-to-high bandwidths. A choice of Silicon, Germanium or InGaAs offers operation at a variety of wavelengths.

Another important consideration is the size of the detector or the active area. Active area corresponds to the size of the actual light sensitive region, independent of the package size. PIN Diodes with large active areas will capture more light but will

always be slower than smaller devices and will also produce more noise. However, if a small device contains an attached lens it will often collect as much light as a much larger device without a lens. However, the devices with attached lenses will collect light over narrower incident angles (acceptance angle). Flat surface devices are usually used if light must be detected over a wide area. For most applications either style will work. For high speed applications a device with a small active area is always preferred. However, there is a tradeoff between device speed and the active area. For most long-range applications, where a large light-collecting lens is needed, a large area device should be used to keep the acceptance angle from being too small. Smaller acceptance angles can make it nearly impossible to point the receiver in the right direction to collect the light from the distant transmitter.

3.4 ALIGNMENT PROBLEM

Continuous alignment between transmitter and receiver during communication is essential for the successful data transmission. This is particularly problematic when narrow beam divergence angles and fields of view (FOVs) are used. Thermal expansion of building frame parts and weak earthquakes are the possible causes of misalignment [1]. Another common cause of misalignment is wind, especially when communication equipment is placed on tall buildings. Under the influence of dynamic wind loads, many high-rise buildings sway in along-wind and across-wind directions, or twist due to torsion. This interrupts the line-of-sight. The horizontal movement of the building due to these effects can vary from 1/200 to 1/800 of the building height. Building sway is a random process that affects system performance since it is a source of pointing error at the beam steering stage. Knowledge of the stochastic behavior of the pointing error enables corrective transceiver design or solutions on the system level such as intelligent protocols.

3.5 SCATTERING

It is generally agreed that the primary drawback of OWC system is the downtime that results from adverse weather conditions. Although rain and snow can hamper light propagation, the most detrimental environmental conditions are fog and haze. This is due to their high concentration of scattering particles with radii of the same order of magnitude as the laser wavelength [1]. Scattering is the deflection of incident light from its initial direction, which causes spatial, angular, and temporal

spread. The precise scattering mechanism is dependent on the ratio of particle size to radiation wavelength. When this ratio is near to unity, the direction of propagation subsequent to scatter is determined by the Mie-scattering solution to the Maxwell wave equation. Given the size distribution of the scattering particles, the wavelengths of radiation, and the refractive indices of both the drop and the air, the probability function of the Mie-scattering angle can be derived. Hence, the scattering and resultant communication degradation can be predicted. Raindrops and snowflakes are very much larger than optical wavelengths, and are not subject to Mie-scattering and do not seriously impede light propagation. Scattering results in attenuation and distortion of the transmitted signal. Attenuation of the order of tens or even hundreds of decibels per kilometer can be encountered when the propagation channel is unfavorable.

3.6 ABSORPTION

Molecules in the atmosphere absorb laser light energy, causing attenuation of the optical power [1]. This phenomenon is extremely sensitive to wavelength so that a given environment may be transparent to some wavelengths, while almost entirely blocking others. The infrared absorption by the atmosphere is largely due to water vapor and CO_2, while below around 200 nm absorption by O_2 and O_3 are so high that there is virtually no transmission. Regions of fair transmission are called *free absorption windows*, and are found in the visible and near infrared range. At middle infrared wavelengths there are more absorption windows in the region of 3–5 μm and 8–12 μm, but above 22 μm the water vapor absorption again rises to prohibitive levels for transmission. Weather can often change rapidly, and as the molecular content of the atmosphere alters, the transmission characteristics of the propagation channel change too. These changes are due to absorption as well as scattering and may seriously influence the availability of a link. Paradoxically, the absorption of the transmitted signal can be seen as an advantage when strict security is a priority, as beyond a limited range no power can be detected.

3.8 TURBULENCE

Turbulence effects are due to varying temperatures and humidity levels within the propagation media. It causes scintillation of the light and "beam wander" [6]. In other words, the amplitude of the received signal fluctuates over time, and the

position of the incident light shifts in space. This may be due to air conditioning vents in the vicinity of the transceiver, irradiative heat from the roof or currents of pollutants in the atmosphere. Temperature and humidity gradients cause changes in the atmospheric refractive index, which is the source of optical distortions. Winds and cloud coverage also influence the level of turbulence, and even the time of day can alter temperature gradients, and hence turbulence effects. A number of statistical models have been developed to describe the dependence of the refractive index on the ambient temperature, pressure, and humidity as well as on the radiation wavelength. The basic statistical parameter commonly used for analyzing power transmission is the spatial cross-correlation of the randomly varying refractive index. The power spectral density of the index fluctuations defined for spatial frequency is the three-dimensional Fourier transform of the spatial cross-correlation function. To model turbulence, different energy exchange mechanisms have been distinguished, corresponding to different ranges of spatial frequency. Commonly, the strength of the turbulence is described using the auxiliary term C_n^2 (the refractive index structure constant) where inertial forces dominate. This inertial range of spatial frequencies is called the *Kolmogorov spectrum* and has been extensively investigated both theoretically and empirically. Using Ritov theory, a lognormal power intensity distribution function has been derived for the spatial distribution of light propagation through a turbulent atmosphere.

In this chapter, the major design challenges in outdoor optical wireless link have been briefly discussed. In the next chapter, the theory of radiative transfer and scattering is discussed in detail. Also, the various distributions available for rain, fog and smog are discussed.

CHAPTER 4
THEORETICAL STUDY OF OUTDOOR OPTICAL WIRELESS LINKS IN RAIN, FOG AND SMOG

4.1 THE ATMOSPHERIC CHANNEL

The atmosphere is composed of collections of gases, atoms, water vapor, pollutants and other chemical particulates that are trapped by the Earth's gravity field and it extends to approximately 400 miles in altitude. The heaviest concentration of these particles is near Earth in the troposphere level with particle density decreasing with altitude up through the ionosphere. Actual particle distribution depends on the atmospheric conditions. These atmospheric particles interact with all radiation fields that propagate through the radiation belts, with the primary effects being power losses and wavefront distortion.

Power losses and distortion are caused by the absorption and scattering of the radiation fields by the particulates. These effects become most severe as the radiation wavelengths begin to approach the cross-sectional dimension of the particulates. Because particle sizes in the atmosphere range from centimeters down to micrometers, the atmosphere is especially deleterious to optical transmissions.

Atmospheric conditions can be roughly classified into three basic types: clear air, clouds and rain. The clear air channel is the most benign, characterized by long range visibility, clear weather and relatively low attenuation. Clear air, however, can still contain eddies and temperature gradients (clear-air turbulence) that can produce changes in the index of refraction of impinging fields. These index changes act as optical lenses that refocus and reorient beam propagation. Cloudy atmospheric conditions can range from mist and fog to heavy cloud cover extending from near Earth to upper altitudes and is characterized with increasing water vapor accumulation and higher levels of attenuation. Rain represents the presence of water droplets of significant sizes, and can produce the severe effects, depending on rainfall rate and rain cloud extent.

As field radiation impinges on an atmospheric particulate, a portion of its energy is absorbed, and the angle of the remainder is redirected. The particle absorption produces

a field power loss and the angle redistribution produces scattered energy. Surrounding particles further absorb and scatter the redistributed field, producing aggregate field attenuation and scattering mechanism on the overall field as it propagates. It is precisely this scattering within a sunlit cloud, for example, that makes it appear uniformly illuminated when observed from below.

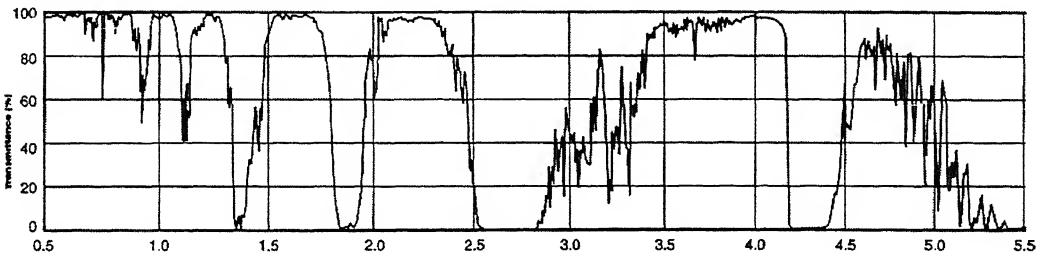

Figure 4.1 Transmittivity of the atmosphere [2]

Figure 4.1. shows a plot of the field transmittance observed at various optical wavelengths propagating through the clear air atmosphere. The significant attenuation observed at selective wavelengths indicates field absorption from specific particles and shows the importance of properly selecting wavelengths in the high transmittive bands for space optics systems.

The important parameters that represent the atmospheric conditions are the particle size (cross sectional dimension relative to the wavelength), and the particle density (volumetric concentration of particles). Low densities of large particles tend to obey single scatter theory and produce primarily attenuation with mostly forward scattering at angles close to the normal. High densities of small particles tend to obey multiple scatter theory, which produce elemental beam scattering and random phase shifting across the wave-front as it propagates.

Figure 4.2 shows typical values for average particle size and the corresponding particle densities for various cloud and rain conditions. It is evident from the figure that the conditions vary from high density small particles during mist and fog to low-density large-particle concentrations during heavy rain.

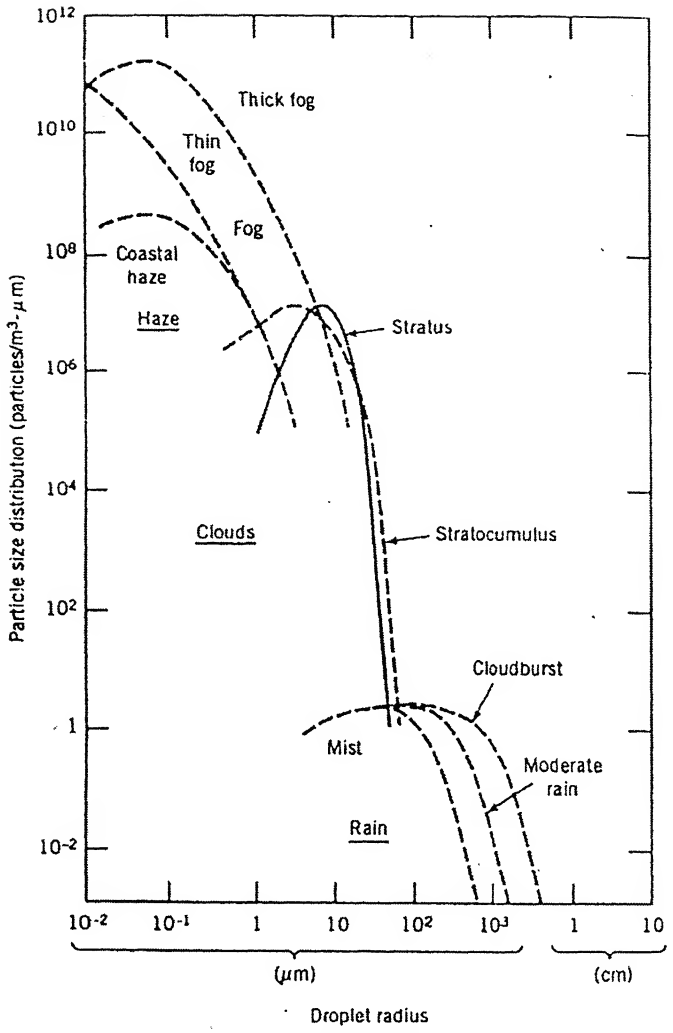

Figure 4.2 Cloud and precipitation drop size distribution [2]

The different types of atmospheric constituent's sizes and concentrations can be tabulated as:

Type	Radius (μm)	Concentration (cm^{-3})
Air Molecules	10^{-4}	10^{19}
Aerosol	10^{-2} to 1	10 to 10^{3}
Fog	1 to 10	10 to 100
Cloud	1 to 10	10 to 300
Raindrops	10^{2} to 10^{4}	10^{-5} to 10^{-2}

Table 4.1 Atmospheric constituents, their sizes and concentrations [12]

4.2 ATMOSPHERIC CONDITIONS

Under different atmospheric conditions, an optical wireless communication system undergoes different attenuation in accordance with the theory of radiative transfer (to be discussed in the following section). The attenuation can vary from 0.4 dB/km to 500 dB/km, depending upon the weather conditions. The laser beam propagating through the atmosphere is attenuated by scattering and absorption of radiation by the following atmospheric conditions:

1. Rain
2. Fog
3. Smog
4. Dust

The impact of the various weather conditions on an OWC link is shown in Fig 4.3. It can be seen that in heavy fog, the attenuation over a link can be a few hundreds of dB/km, whereas that for rain it is a few tens of dB/km.

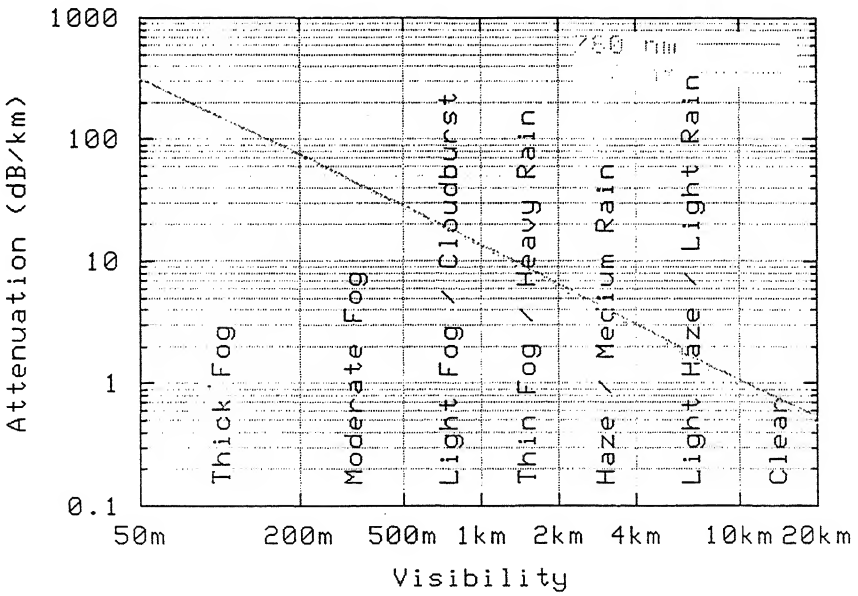

Figure 4.3 Impact of weather on laser power

4.3 SCATTERING

When a beam of light impinges on a particle, electric charges in the particles are excited into an oscillatory motion. The excited electric charges reradiate energy in all directions (scattering) and may convert a part of the incident radiation into thermal energy (absorption) [16] and [17].

The energy scattered by a particle (F_{scat})is proportional to the incident intensity F_i and is given by,

$$F_{scat} = C_{scat}Fi \tag{4.1}$$

where C_{scat} has units of m^2, is the single-particle scattering cross section. For absorption, the energy absorbed (F_{abs}) is described analogously as,

$$F_{abs} = C_{abs}Fi \tag{4.2}$$

where C_{abs} in units of m^2, is the single-particle absorption cross section.

Conservation of the energy requires that the light removed from the incident beam by the particle is accounted for by scattering in all directions and absorption in the particle. The combined effect of scattering and absorption is referred to as extinction, and an extinction cross section C_{ext} can be defined by

$$C_{ext} = C_{scat} + C_{abs} \tag{4.3}$$

The dimensionless scattering efficiency of a particle Q_{scat}, is C_{scat}/A, where A is the cross-sectional area of the particle. Defining Q_{abs} and Q_{ext} in the same way,

$$Q_{ext} = Q_{scat} + Q_{abs} \tag{4.4}$$

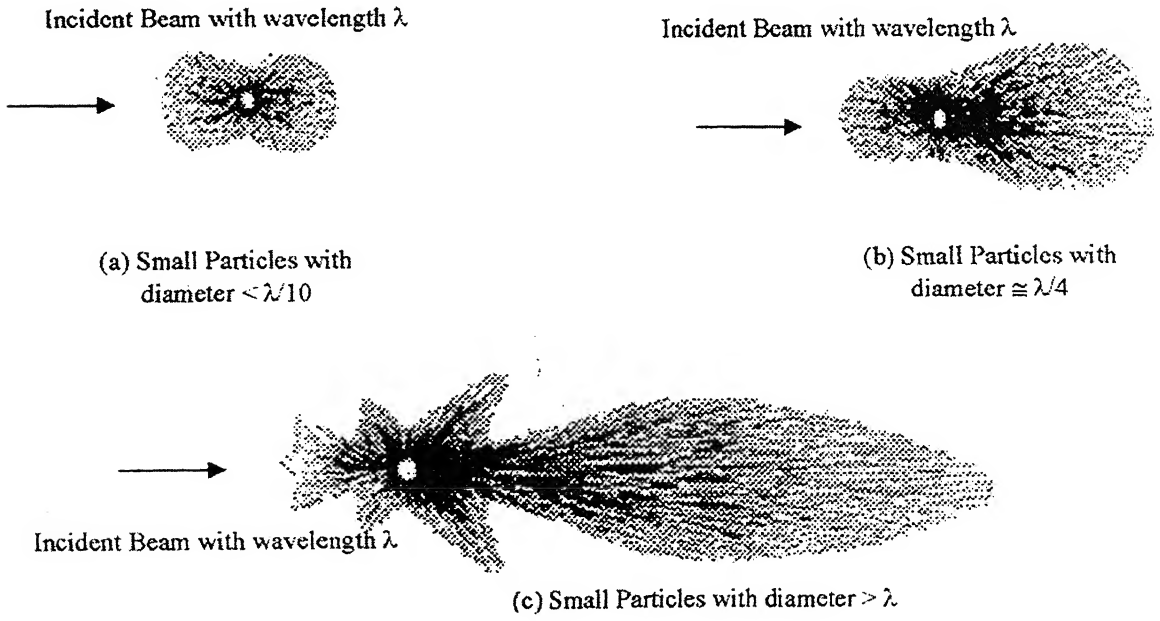

Figure 4.4 Scattering patterns of electromagnetic waves by spherical drops
(a) Rayleigh Scattering (b) Mie Scattering (c) Geometric Scattering [24]

Light scattering mechanisms of the particle can be divided into three categories depending upon the size parameter x (which is equal to $2\pi r/\lambda$, where r is the radius of the particle) and the wavelength :

1. Rayleigh Scattering
2. Mie Scattering
3. Geometric Scattering

4.3.1 Rayleigh Scattering

When the particle is much smaller than the wavelength of the incident light, Rayleigh scattering takes place [25]. With respect to light in the visible range of the spectrum, particles of diameter < 0.1 μm lie in the Rayleigh scattering regime. In this regime the pattern of scattered light intensity is symmetrical in the forward and backward directions and more or less independent of particle shape. Rayleigh scattering occurs primarily off the gaseous molecules in the atmosphere. The attenuation coefficient varies as λ^{-4} (where λ is the wavelength).

Incident light on a particle having very small size compared to the wavelength, behaves in the same way as if the particle is placed in a homogeneous electric field. The particle's own field, caused by the electric polarization of the particle, modifies this field both inside and near the particle. This induces a dipole moment. The oscillating dipole radiates in all directions. This type of scattering is called Rayleigh scattering.

Two conditions required for Rayleigh scattering are:

1. Size of the particle should be small compared to the wavelength.
2. The applied field should penetrate so fast into the particle that the static polarization is established in a time short compared to the period.

For an incident wave of unit density, the intensity of the scattered wave at a distance l from the particle is given by [25]

$$I_{scat} = \frac{16\pi^4 r^6}{l^2 \lambda^4} \left(\frac{\varepsilon_1 - \varepsilon_2}{\varepsilon_1 + 2\varepsilon_2} \right)^2 \sin^2 \psi \qquad (4.5)$$

or

$$I_{scat} = \frac{16\pi^4 r^6}{l^2 \lambda^4} \left(\frac{m^2 - 1}{m^2 + 2} \right)^2 \sin^2 \psi \tag{4.6}$$

where m is the refractive index, λ is the wavelength in the medium and ψ is the angle measured from the scattering direction to the dipole.

The extinction and scattering efficiencies for particles in the Rayleigh scattering regime are given by [25]

$$Q_{ext}(m,x) = 4x \operatorname{Im}\left\{ \frac{m^2 - 1}{m^2 + 2} \left[1 + \frac{x^2}{15} \left(\frac{m^2 - 1}{m^2 + 2} \right) \frac{m^4 + 27m^2 + 38}{2m^2 + 3} \right] \right\} + \frac{8}{3} x^4 \operatorname{Re}\left\{ \left(\frac{m^2 - 1}{m^2 + 2} \right)^2 \right\} \tag{4.7}$$

and

$$Q_{scat}(m,x) = \frac{8}{3} x^4 \left| \frac{m^2 - 1}{m^2 + 2} \right|^2 \tag{4.8}$$

4.3.2 Mie Scattering

As the particle size approaches the laser wavelength, the scattering of radiation off the larger particle becomes more dominant in the forward direction as opposed to the backward direction [25]. This type of scattering, where the size parameter x varies between 0.1 and 50 is called the Mie scattering. The lasercom wavelengths are Mie scattered by haze and smaller fog particles. The detailed explanation of Mie Scattering is given in section 4.6.

4.3.3 Geometric Scattering

When the particle size parameter x is greater than 50, the scattering is called geometric or non-selective scattering [25]. This type of scattering is strongly dependent on the particle shape and orientation relative to the incoming beam. The scattering is called non-selective because there is no dependence of the attenuation coefficient on laser wavelength.

The fundamental fact is that the incident beam of light, which forms a plane wavefront of infinite extent, may be thought to consist of separate rays of light which pursue their own path. A small part of a wide wavefront can be looked upon as defining a ray which has for some length its own existence independent of the entire wavefront. A

length l requires a width of the order of $\sqrt{(l\lambda)}$, and the requirement for any separate existence at all is a width > λ. For a particle with a size of 20 or more times the wavelength, it is possible to distinguish fairly sharply between the rays incident on the particle and the rays passing along the particle. Among the former it is possible to distinguish rays hitting various parts of the particle's surface.

The rays hitting the particle and passing along it give rise to two distinct phenomena:

1. Reflection and Refraction

   Rays hitting the particle's surface are partially reflected and partially refracted. Refracted light may emerge after another refraction, or after several internal reflections. The light so emerging and the light directly reflected from the outer surface both contribute to the total *scattering* by the particle. The energy that does not emerge is lost by absorption inside the particle.

2. Diffraction

   The rays passing along the particle forms a plane wavefront from which a part, in the form and size of the geometrical shadow of the particle, is missing. This incomplete wavefront gives rise to a certain angular distribution of intensity, called the Fraunhoffer diffraction pattern.

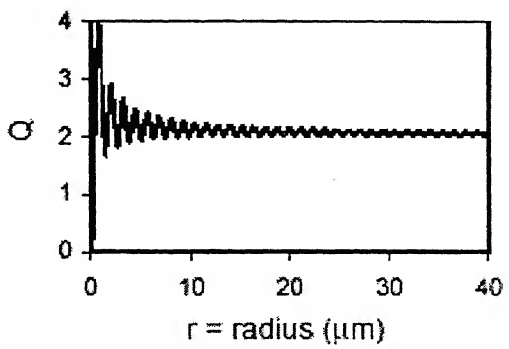

Figure 4.5 Scattering efficiency of water particles scattering
785 nm light as a function of particle size

As the particle size increases, the value of Q_{ext} approaches to 2. The reason for this is as follows. The efficiency represents the ratio of energy removed from the wave to the total energy intercepted by it. All energy falling on the particle is scattered or absorbed, i.e., in any event removed from the proceeding wave. This gives an effective cross-

section equal to G, the geometric area. Besides that we have the diffraction forming an angular pattern that is identical with the diffraction through a hole of area G by Babinet's principle. This gives diffraction with a cross-section G. The total energy removed from the proceeding wave corresponds to a cross-section $2G$, i.e., to an efficiency factor $Q_{ext} = 2$.

4.4 RADIATIVE TRANSFER

The basis of classical transfer theory is the Lambart Bouger law, which states that the change in intensity of radiation due to an interaction with matter depends directly on both the incident intensity and the amount of matter [26]. A beam or pencil of radiation is attenuated by its interaction with the medium through which it passes. If the initial intensity is I, then after traveling distance ds along the direction of propagation, the change in the intensity will be

$$dI = -k_{ext}(s)\rho I ds = -\beta_{ext}(s) I ds \tag{4.9}$$

The parameter ρ is the density (g/cm^3) of the attenuating medium. Equation (4.9) defines the mass extinction coefficient k_{ext} and the volume extinction coefficient β_{ext}. β_{ext} has the dimensions of cm^{-1}, and k_{ext} have the dimensions cm^2/g.

The theory also assumes that emission by an element of mass or volume is linear in both intensity and the amount of matter present. The net increase in intensity in a distance ds along the direction of propagation is $\varepsilon(s)ds$. The equation of transfer for a given path through a medium can be thus expressed as

$$\frac{dI(s)}{ds} = -\beta_{ext}(s) I(s) + \varepsilon(s) \tag{4.10}$$

Formal integration of this one-dimensional transfer equation of the path from s = 0 to s = S gives

$$I(s) = I(0)e^{-\tau} + \int_0^S \varepsilon(s')e^{-(\tau-\tau')}ds' \tag{4.11}$$

in which the optical thickness along the path is τ

$$\tau = \int_0^S \beta_{ext}(s)ds$$
$$\tau' = \int_0^{s'} \beta_{ext}(s'')ds'' \tag{4.12}$$

This formal solution to the equation shows that the resultant intensity is the sum of two distinct terms; the incident intensity attenuated by extinction along the path (0,S) and a component due to emission at points along the path, attenuated along the path (s',S). If we neglect the emission term, we have the usual form of Lambart-Bouger law.

$$I(R) = I(0)\exp(-\beta_{ext} R) \tag{4.13}$$

where β_{ext} is the mean value over the path and R is the distance over which the intensity reduction is to be calculated.

Beer–Lambert Law

The alternative form of the radiative transfer theory is the Beer-Lambart law also known as Beer's law or the Beer-Lambart-Bouger law. This law is an empirical relationship in relating the extinction of light to the properties of the material the light is traveling through.

It states that the extinction coefficient $\beta(\lambda)$, of a species at a particular wavelength of electromagnetic radiation λ, is proportional to the concentration c of the scattering or absorbing species, of the electromagnetic radiation through the sample containing the absorbing species. This can be written in the form:

$$\beta(\lambda) = \sigma(\lambda)c \tag{4.14}$$

The proportionality constant $\sigma(\lambda)$ is called the extinction cross section of the species at the wavelength λ.

The value of the extinction coefficient β varies between different absorbing and scattering materials and also with wavelength for a particular material. It is usually determined by experiment.

The law tends to break down at very high concentrations, especially if the material is highly scattering. If the light is especially intense, nonlinear optical processes can also cause variances.

Extinction coefficient is a measure of the amount of radiated power absorbed and scattered. Mathematically,

$$\beta(\lambda) = \log(P_0 / P)$$

where P_0 is the incident power and P is received power.

Hence, Beer law alternatively can be stated as

$$P(R) = P(0)\exp(-\sigma cl)$$

$$P(R) = P(0)\exp(-\beta_{ext} l) \tag{4.15}$$

4.5 VISIBILITY

This is an important parameter needed to calculate the optical attenuation due to Fog, Haze and clouds. Visibility is generally expressed as a distance. It is defined as the maximum distance at which the object contrast against its background is 2% using 550nm wavelength light that the human eye is most sensitive to. If the contrast at a distance z is *C(z)*, then the relative contrast, defined as the ratio of *C(z)/C(0)* can be expressed as [27].

$$\frac{C(z)}{C(0)} = \left(\frac{L_{\max}(z) - L_{\min}(z)}{L_{\min}(z)}\right)\left(\frac{L_{\min}(0)}{L_{\max}(0) - L_{\min}(0)}\right) \tag{4.16}$$

where $L_{max}(z)$ refers to the object luminance and $L_{min}(z)$ is background luminance at distance z. The value of z for $\frac{C(z)}{C(0)} = 0.02$ is called the visual range (V). If we assume the background irradiance to be zero at z=0 and z=z, then Eqn.(3.28) reduces to

$$\frac{C(z)}{C(0)} = \frac{L_{\max}(z)}{L_{\max}(0)}$$

From Ref [27] we see that $L_{max}(z)$ can be approximated as

$$L_{\max}(z) = L_{\max}(0)\exp(-\beta_{ext} s)$$

where α is the attenuation coefficient.

Hence at visual range (i.e. at s=V) we get

$$\frac{C(V)}{C(0)} = \exp(-\beta_{ext} V) = 0.02$$

Hence

$$\beta_{ext} V = -\ln(0.02) = 3.912$$

Substituting, we get V in kilometers as

$$V = \frac{|\ln(0.02)|}{\beta_{ext}(\lambda = 550nm)} = \frac{3.912}{\beta_{ext}(\lambda = 550nm)} \text{ km} \tag{4.17}$$

If the visibility for an outdoor optical link is given, then the extinction coefficient can be calculated using the following equation

$$\beta = \frac{3.91}{V}\left(\frac{\lambda}{0.55\mu m}\right)^{-q} \tag{4.18}$$

where q = 1.6 for good visibility i.e. V > 50 km,

q = 1.3 for 6 km < V < 50 km,

q = 0.585 $V^{1/3}$ for V < 6 km

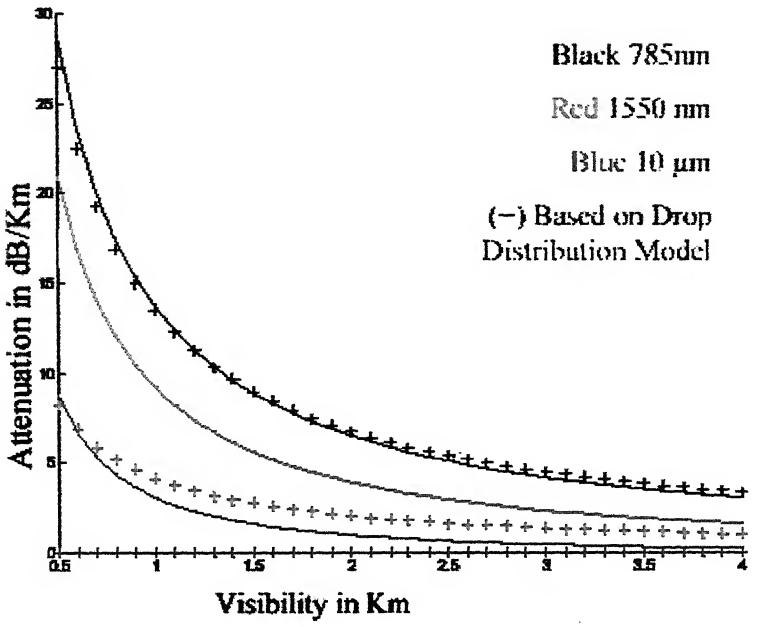

Figure 4.6 Attenuation versus visibility [13]

If we look at Fig 4.4, we will find that the attenuation value based on equation 4.18 is higher than the value calculated by using the drop distribution model. It is due to the independence of, exponent value and the one-to-one relation between visibility and attenuation coefficient, from droplet sizes and distributions. As the drop size distribution varies from place to place, the value of attenuation can not be same.

To calculate the attenuation coefficient accurately, one can make use of the Mie-Debye theory (discussed in the next section).

4.6 MIE-DEBYE THEORY

Mie Debye theory is the rigorous treatment of electromagnetic wave scattering by spherical particles in a surrounding medium [28].

Assumptions made while using Mie Debye theory:

1. Particle is a sphere.
2. Particle is homogeneous (therefore it is characterized by a single refractive index m = n-ik at a given wavelength).

The size parameter in Mie theory is defined by $x = 2\pi r/\lambda$ where r is the radius of drop and λ is the wavelength of incident light in the medium. Relative refractive index of the sphere is $m = n_{sphere} / n_{medium}$ with n_{sphere} the complex refractive index of the sphere and n_{medium} that of the medium. Mie coefficients are expressed as

$$a_n = \frac{\psi_n'(mx)\psi_n(x) - m\psi_n(mx)\psi_n'(x)}{\psi_n'(mx)\zeta_n'(x) - m\psi_n(mx)\zeta_n'(x)} \tag{4.19}$$

$$b_n = \frac{m\psi_n'(mx)\psi_n(x) - \psi_n(mx)\Psi_n'(x)}{m\psi_n'(mx)\zeta_n(x) - \psi_n(mx)\zeta_n'(x)} \tag{4.20}$$

where $\psi_n(x) = xj_n(x)$ and $\zeta_n(x) = xh^{(2)}{}_n(x) = x(j_n(x) - in_n(x))$ are the Ricatti-Bessel functions with the following properties,

$$\psi_{n+1}(x) = (2n+1)\psi_n(x)/x - \psi_{n-1}(x) \tag{4.21}$$

$$\zeta_{n+1}(x) = (2n+1)\zeta_n(x)/x - \zeta_{n-1}(x) \tag{4.22}$$

$$\psi_n'(x) = \psi_{n-1}(x) - n\psi_n(x)/x \tag{4.23}$$

$$\zeta_n'(x) = \zeta_{n-1}(x) - n\zeta_n(x)/x \tag{4.24}$$

$$\psi_{-1}(x) = \cos(x) \tag{4.25}$$

$$\psi_0(x) = \sin(x) \tag{4.26}$$

$$\zeta_{-1}(x) = \cos(x) + i\sin(x) \tag{4.27}$$

$$\zeta_0(x) = \cos(x) - i\sin(x) \tag{4.28}$$

The index runs from n = 1 to infinity, but the infinite series in Mie formulas can be truncated to a maximum n_{max}, as proposed by Bohren and Huffman,

$$n_{max} = 2 + x + 4x^{1/3}$$

The scattering amplitude functions are

$$S_1(\Theta) = \sum_{n=1}^{\infty} \frac{2n+1}{n(n+1)} \left[a_n\pi_n(\cos\Theta) + b_n\tau_n(\cos\Theta)\right] \tag{4.29}$$

$$S_2(\Theta) = \sum_{n=1}^{\infty} \frac{2n+1}{n(n+1)} \left[b_n\pi_n(\cos\Theta) + a_n\tau_n(\cos\Theta)\right] \tag{4.30}$$

where π_n and τ_n are Mie angular coefficients.

$$\pi\ (\cos\Theta) = \frac{1}{\sin\Theta} P^{1}{}_{n}(\cos\Theta) \tag{4.31}$$

$$\tau\ (\cos\Theta) = \frac{d}{d\Theta} P^{1}{}_{n}(\cos\Theta) \tag{4.32}$$

where $P^{1}{}_{n}$ are the associated Legendre Polynomial.

From equation 4.26,

$$P^{1}{}_{n}(\cos\Theta) = -\frac{dP_n(\cos\Theta)}{d\Theta} = \sin\Theta\pi_n(\cos\Theta)$$

and by differentiation

$$\frac{dP_n(\cos\Theta)}{d\Theta} = \cos\Theta\pi_n(\cos\Theta) - \sin^2\Theta\pi'_n(\cos\Theta) = \tau_n(\cos\Theta) \tag{4.33}$$

The recurrence relations of Legendre polynomials are

$$P_n(\cos\Theta) = \cos\Theta\left[\frac{2n-1}{n-1}\right]P_{n-1}(\cos\Theta) - \left[\frac{n}{n-1}\right]P_{n-2}(\cos\Theta) \tag{4.34}$$

$$P'_n(\cos\Theta) = (2n-1)P_{n-1}(\cos\Theta) + P'_{n-2}(\cos\Theta) \tag{4.35}$$

For the far field zone, the solution of the vector wave equation can be obtained as

$$\begin{bmatrix} E^s_l \\ E^s_r \end{bmatrix} = \frac{\exp(-ikr + ikz)}{ikr} \begin{bmatrix} S_2(\Theta) & 0 \\ 0 & S_1(\Theta) \end{bmatrix} \begin{bmatrix} E^i_l \\ E^i_l \end{bmatrix} \tag{4.36}$$

where E^i_l and E^i_r are the parallel and perpendicular components of the incident electric field, and E^s_l and E^s_r are the parallel and perpendicular components of the scattered electric field.

The scattered far field for a unit amplitude incident field (where the time variation exp(iωt) has been omitted)is given by

$$E^s_l = \frac{\exp(-ikr)}{ikr}\cos(\phi)S_2(\cos\Theta) \tag{4.37}$$

$$E^s_r = \frac{\exp(-ikr)}{-ikr}\sin(\phi)S_1(\cos\Theta) \tag{4.38}$$

Intensity for the natural light of unit intensity

$$I = \frac{\lambda^2{}_2}{8\pi^2 r^2}(i_1 + i_2) \tag{4.39}$$

where $i_1 = \left|S_1(\Theta)^2\right|$ and $i_2 = \left|S_2(\Theta)^2\right|$ are the intensity functions.

Mie efficiency factors are derived from the Mie scattering amplitude

$$Q_{ext} = \frac{2}{x^2}\sum_{n=1}^{\infty}(2n+1)\,\mathrm{Re}[a_n + b_n] \tag{4.40}$$

$$Q_{scat} = \frac{2}{x^2}\sum_{n=1}^{\infty}(2n+1)[|a_n|^2 + |b_n|^2] \tag{4.41}$$

$$Q_{abs} = Q_{ext} - Q_{scat} \tag{4.42}$$

where Q_{ext}, Q_{scat} and Q_{abs} are the extinction efficiency, scattering efficiency and absorption efficiency respectively. As x --> ∞, the extinction efficiency Q_{ext} approaches to a constant value 2.

The coefficients of extinction, scattering and absorption can be calculated from the corresponding Mie efficiencies and the size distribution [28]

$$\beta_j = 0.25\pi\int_0^{\infty} D^2 Q_j(D) N(D) dD \tag{4.43}$$

where D is the diameter of the drop and $N(D)$ is the drop size distribution for the rain/fog/haze.

4.7 RAIN

Attenuation due to rain is an important problem for infrared communication at higher frequencies. In monitoring rainfall and predicting the rain attenuation, the raindrop-size distribution plays an important role.

There are many raindrop size distributions proposed from time to time. We analyzed the attenuation due to the rain using the raindrop size distributions, which is proposed in the literature.

4.7.1 Size Distributions for the rain

Laws and Parsons Distribution

One of the earliest distributions on the size of raindrops was given by Laws and Parsons (LP). They proposed the median diameter D_m:

$$D_m = 1.238R^{0.182}$$

where R is the precipitation rate in millimeter per hour.

This distribution has been found to be a reasonable choice for a mean drop-size spectrum in continental temperate rainfall, though for rain-rates below 35mm/hr. The LP drop size distribution density was fitted to the distribution given by Marshall and Palmer (discussed in the next section).

$$N(D) = 8.0 \times 10^{6} \exp(4100\, R^{-0.21} D)$$

where D is in meter and R is in mm/hr

Two problems were associated with the above equation are shown below:

1. Olsen et al. [29] indicated that it is not consistent with the evaluation of the rain rate.
2. Wolf [30] found that it predicts a maximum value for droplets of zero diameter.

Wolf [30] proposed a new distribution, which fitted more accurately with the LP data and is found to be valid for rain rates of the order of 150 mm/hr.

The new Laws and Parsons distribution proposed is:

$$N(D) = 1.98 \times 10^{7}\, R^{-0.384}\, D^{2.93} \exp(-5.38\, R^{-0.186} D) \qquad (4.44)$$

where D is in millimeters and R in mm/hr.

Marshall and Palmer distribution

Marshall and Palmer [29] proposed a negative exponential form for the average spectrum of drop sizes measured in most rains

$$N(D) = N_0 \exp(-\Lambda D), \qquad \Lambda = \alpha R^{-\beta} \qquad (4.45)$$

where N_0, α and β are constants.

It has been found to be applicable to widespread rain in continental temperate climates, although it has a tendency to overestimate the number of small drops.

The parameters for the above distribution are:

$$N_0 = 0.08\ cm^{-4} \text{ and } \Lambda = 41\, R^{-0.21}\ cm^{-1}$$

where R is the rain rate in mm/hr.

Thunderstorm distribution

Joss et al. [29] classified the rain fall into three types, namely, drizzle (J-D), widespread (J-W) and thunderstorm (J-T). They proposed a negative exponential distribution

$$N(D) = N_0 \exp(-\Lambda D), \qquad \Lambda = \alpha R^{-\beta} \tag{4.46}$$

with the parameters $N_0 = 0.014$ cm^{-4} and $\Lambda = 30\ R^{-0.21}$ cm^{-1}.

This negative exponential distribution was fitted to the average drop size measured in convective rain.

Drizzle Distribution (J-D)

This negative exponential distribution is obtained by fitting the average drop size spectrum of very light widespread rain, or drizzle, composed mostly of small drops. Parameters for this distribution are $N_0 = 0.3$ cm^{-4} and $\Lambda = 57\ R^{-0.21}$ cm^{-1}.

Widespread Distribution (J-W)

This negative exponential distribution is obtained by fitting the average drop size spectrum of very widespread rain. Parameters for this distribution are $N_0 = 0.07$ cm^{-4} and $\Lambda = 4.1\ R^{-0.21}$ cm^{-1}. This distribution can be directly obtained by Marshall and Palmer distribution as the parameters are identical. Consequently, the values of J-W is equal to 7/8 of those for the MP distribution.

Weibull Drop size Distribution

Jiang et al. [31] indicated that the LP distribution's behavior is incorrect for very small drops. They proposed Weibull distribution which incorporate drizzle, widespread rain and shower rain cases.

$$N(D) = N_0 \frac{c}{b}\left(\frac{D}{b}\right)^{c-1} \exp\left\{-\left(\frac{D}{b}\right)^{c}\right\} \tag{4.47}$$

where D is the diameter in mm, $N_0 = 1000$ m^{-3}, $c = 0.95R^{0.14}$ and $b = 0.26R^{0.44}$ mm.

All the raindrop distribution model talked about till now have been based on the temperate regions of the world. The need for the drop size distribution for tropical regions was realized and some more models were proposed for the same.

Log-normal Distribution

Ajayi and Olsen [32] pointed out that the MP distribution frequently used for scattering applications is inadequate for tropical regions. It overestimates the drop number density in the small diameter range at all rain rates, and in the large diameter range at all rain rates, and in the large diameter range (above the mode) at high rain rates.

They proposed a log-normal distribution

$$N(D) = \frac{N_T}{\sigma D\sqrt{2\pi}} \exp\left\{-\frac{1}{2}\left(\frac{\ln D - \mu}{\sigma}\right)^2\right\} \tag{4.48}$$

where μ is the mean of ln D, σ is the standard deviation, and N_T is the total number of drops of all sizes.

The parameters are:

$N_T = 108\ R^{0.363}$,

$\mu = -0.195 + 0.199 \ln R$

$\sigma^2 = 0.137 - 0.013 \ln R$

Maitra [33] conducted experiments in Calcutta and gave the following parameters for the above distribution

$N_T = 54\ R^{0.469}$,

$\mu = -0.538 + 0.0174 \ln R$

$\sigma^2 = 0.0685 + 0.0755 \ln R$

Gamma Distribution

Gamma distribution was originally proposed by Atlas and Ulbrich [31].

$$N(D) = N_0 \exp(-\Lambda D),$$

where $N_0 = 64500\ R^{-0.5}\ m^{-3}\ mm^{-1}$ and $\Lambda = 7.09\ R^{-0.27}\ mm^{-1}$.

This distribution was found not to be matching with the tropical region distribution. So, Ajayi and Olsen [32] proposed a modified gamma distribution for the tropical regions.

$$N(D) = 0.070\ D^{1.43} \exp(-386\ R^{-0.432}\ D^{2.6}), \qquad R \leq 15\ mm/hr \tag{4.49}$$

$$N(D) = 0.056\ D^{1.43} \exp(-895\ R^{-0.515}\ D^{3.1}), \qquad R > 15\ mm/hr \tag{4.50}$$

Maitra [33] mentioned in his paper that only these two parameter model is not adequate for describing the drop size distribution in tropical regions and has proposed a three parameter gamma model.

$$N(D) = N_0 \exp(-\Lambda D),$$
$$= N_T \Lambda^{n+1} D^n \exp(-\Lambda D) / \Gamma(n+1) \quad m^{-3} mm^{-1} \tag{4.51}$$

The parameters are :

$N_T = 564\ R^{0.538}$

$n + 1 = 5.61\ R^{-0.407}$

$\Lambda = 9.18\ R^{-0.387}$

The lognormal gives lower number density for smaller drops than the gamma distribution.

4.8 FOG

Fog presents one of the most important problems to the outdoor optical wireless links. In predicting the attenuation due to fog, the drop-size distribution plays an important role.

4.8.1 Size distribution of fog

Deirmendjian [34] proposed a distribution function of the form

$$n(r) = Ar \exp(-br^\gamma) \tag{4.52}$$

which vanishes at r = 0, ∞ and is called as modified gamma distribution. The four constants A, α, γ and b are positive and real, and α is an integer. They are not independent of each other, and are related to quantities in the frequency distribution, which can be determined by measurements.

Upon integration over the entire range of radii, we get

$$N = A\int_0^\infty r^\alpha \exp(-br^\gamma)dr$$
$$= A\gamma^{-1}b^{-(\alpha+1)/\gamma}\Gamma\left(\frac{\alpha+1}{\gamma}\right) \tag{4.53}$$

which shows that the constant A is essentially given by N, the total number of particles per unit volume. Furthermore, differentiation of equation 4.53 with respect to r yields,

$$\frac{d}{dr}n(r) = Ar^{\alpha-1}\left(\alpha - \gamma br^\gamma\right)\exp\left(-br^\gamma\right) \tag{4.54}$$

which has three zeros, two of which are at r = 0 (provided α > 1) and at r = ∞, respectively. If α = 1, the derivative at the origin is equal to A. The third zero is found by

putting the last factor in equation 4.44 equal to zero, which determines the absolute maximum of the function, whence

$$b = \frac{\alpha}{\gamma\,(r_c)^{\gamma}}$$

with

$$n(r_c) = A\, r_c^{\alpha} \exp\left(-\frac{\alpha}{\gamma}\right)$$

where r_c is the mode radius or size of maximum frequency in the distribution, obtainable from the particle counts. Thus the constant b is determined by r_c provided α and γ are fixed or otherwise obtained from the shape of the experimental distribution curve.

Later, Chu and Hogg [35], modified this distribution, and proposed the following modified form of the distribution

$$n\left(\frac{r}{r_c}\right) = A\left(\frac{r}{r_c}\right)^{\alpha} \exp\left[-b\left(\frac{r}{r_c}\right)^{\gamma}\right] \qquad (4.55)$$

where

$$A = \left(\frac{\alpha}{\gamma}\right)^{(\alpha+1)/\gamma} \frac{\gamma}{\Gamma\left(\frac{\alpha+1}{\gamma}\right)} \frac{N}{r_c} \quad \text{and} \quad b = \frac{\alpha}{\gamma}$$

N is the number of drops per unit volume, r_c is the mode radius of the drops, and α and γ, parameters which can bc adjusted to fit an observed fog particle size distribution.

In figure 4.7 four plots of the above equation are given for several combinations of parameters. Three of these exhibits a slope on the larger drop side of the maximum ($r > r_c$). The other combination of parameters ($\alpha = 2$, $\gamma = 3$) corresponds to the asymptotic distribution of coagulating particles and has a sharp decreasing rate on both sides of the maximum number density. It is of course impossible to have a model for every possible fog distribution, but using the different combinations of α and γ, as shown in the figure 4.7, almost all the atmospheric fogs can be described.

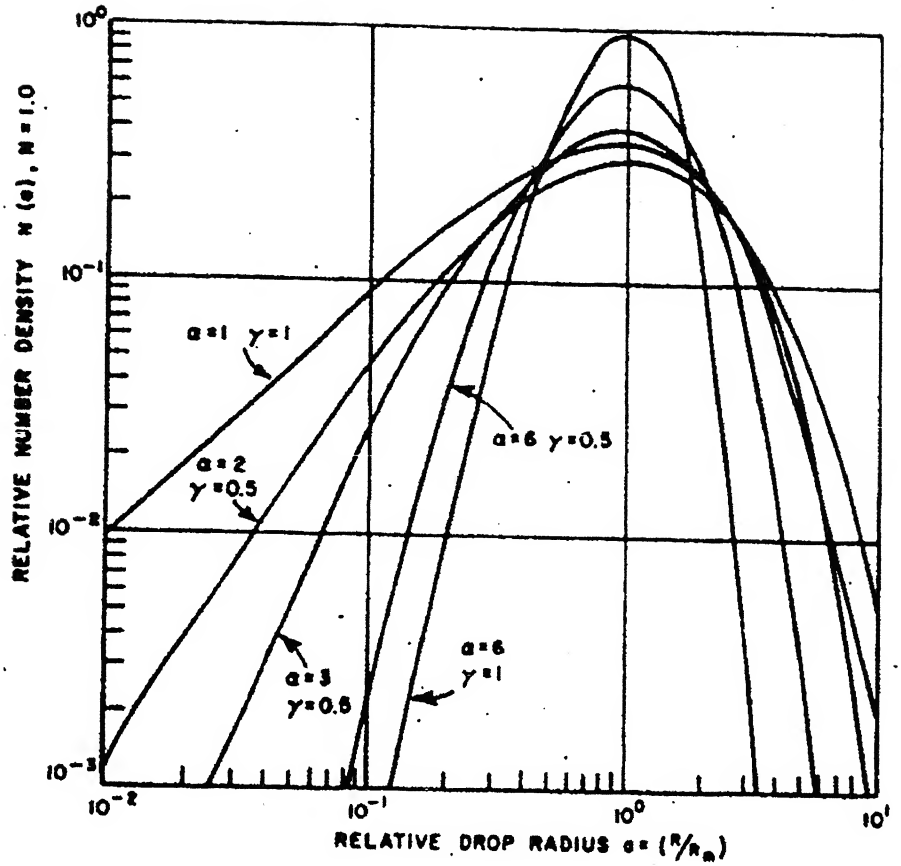

Figure 4.7 Fog model size distribution [35]

Using these model distributions, extinction coefficients have been plotted with respect the radius at maximum number density r_c in figure 4.8 as given in [25]. These curves merge at somewhat smaller values of r_c because the drops larger than r_c contribute more to the extinction than the smaller ones.

The various values of the distributions of the fog and haze for a few α and γ combinations are tabulated below:

Distribution Type	Modal radius (μm)	a	α	γ	b
Heavy Fog	10	0.027	3	1	0.3
Moderate Fog	2	607.5	6	1	3
Light Fog	1	341	2	0.5	4
Haze L (continental)	0.07	5.0e6	2	0.5	15.1

Table 4.2 Distribution model for fog

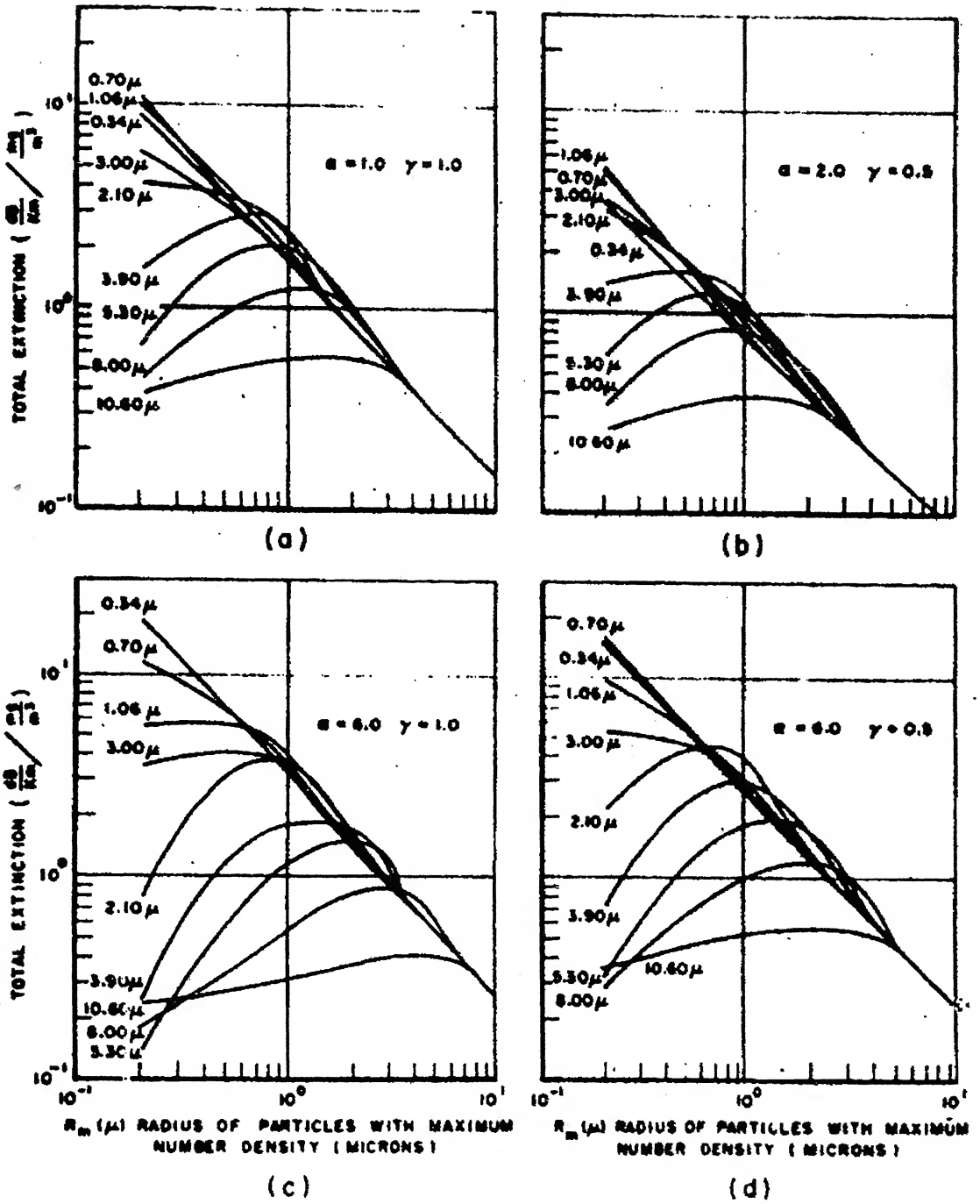

Figure 4.8 Extinction cross section for different drop radius [35]

4.9 SMOG

Another major challenge faced by the outdoor optical link is the attenuation due to smog. Smog is nothing but a mixture of smoke and fog, a colloid system in which the

disperse phase consists of a mixture of gas and moisture and the dispersion medium is air. Major portion of smog-formers come from burning of petroleum-based fuels such as gasoline. Other smog-formers, volatile organic compounds, are found in products such as paints and solvents. Major smog occurrences are often linked to heavy motor vehicle traffic. In short the smog can be defined as the fog having high pollution content. The study of smog is divided into two parts. First the effect of the pollution on the link and the study on the overall effect i.e., smog.

Light extinction due to smoke is made up of the following independent components:

(a) Particles scatter light in a similar way to gases. Scattering is a function of the wavelength of light, particle size and the index of refraction for the particles. Particles of 0.5μm in diameter are the most efficient at scattering light.

(b) Scattering by gases (Rayleigh scattering) which is a constant value for a given temperature and pressure. Molecules of gas in the atmosphere divert light from a sight path.

(c) Gases absorb light and transform it into molecular energy. Nitrogen dioxide concentration is associated with light absorption by gases because absorption by other gas molecules is negligible. But for visible and infrared, there is no molecular absorption as shown in figure 4.9.

(d) Absorption of light by particles occurs when black or colored particles transform light into heat. Absorption is linked to the concentration of elemental carbon in the atmosphere.

A number of studies have shown that different chemical species have differing effects on visibility degradation. Table 4.3 gives the contribution of the species in the degradation of the visibility for visible and near infrared wavelengths. These visibility effects are normally split amongst six main groups which are:

- fine ammonium sulphate
- fine ammonium nitrate
- elemental carbon
- remainder of fine particles (coarse)

Species	% contribution to extinction
Ammonium Sulphate	20.2
Ammonium Nitrate	17.2
Carbon	50
Particulate Mass (Suspended Particles)	6.6
Rayleigh Scattering	6

Table 4.3 Visibility apportionment due to pollution

Following assumptions have been made:

- all components contributing to scattering are included as independent variables
- the components are externally mixed
- scattering efficiency for each component is constant

The particle scattering coefficient can be defined by the sum of the scattering coefficient due to sulphates (b_{SO4}), nitrates (b_{NO3}) and the coarse suspended particles (b_{Coarse}). Thus the particle scattering coefficient can be expressed as:

$$b_{sp} = b_{SO4} + b_{NO3} + b_{Coarse} \tag{4.56}$$

Because certain aerosols, such as sulphates and nitrates, have an affinity for water, their scattering characteristics change as a function of relative humidity (RH). Therefore, scattering of the so-called hygroscopic species as a function of relative humidity must be considered. The adjustment factor for relative humidity is:

$$f(RH) = 0.34 + 0.59(1/(1-RH)) + 0.09(1/(1-RH))^2$$

Each of the particle scattering coefficients can be related to the mass of the components using the following relations:

$$b_{SO4} = 3[Sulfates]f(RH)$$
$$b_{NO3} = 3[Nitrates]f(RH)$$
$$b_{Coarse} = 0.6[Coarse\ Suspended\ particles]$$

The quantities in brackets are the species concentration expressed in $\mu g/m^3$. The numeric coefficients are the dry specific scattering efficiencies (m^2/g). The term *f(RH)* is the relative humidity adjustment factor. The extinction coefficients are in mm^{-1}.

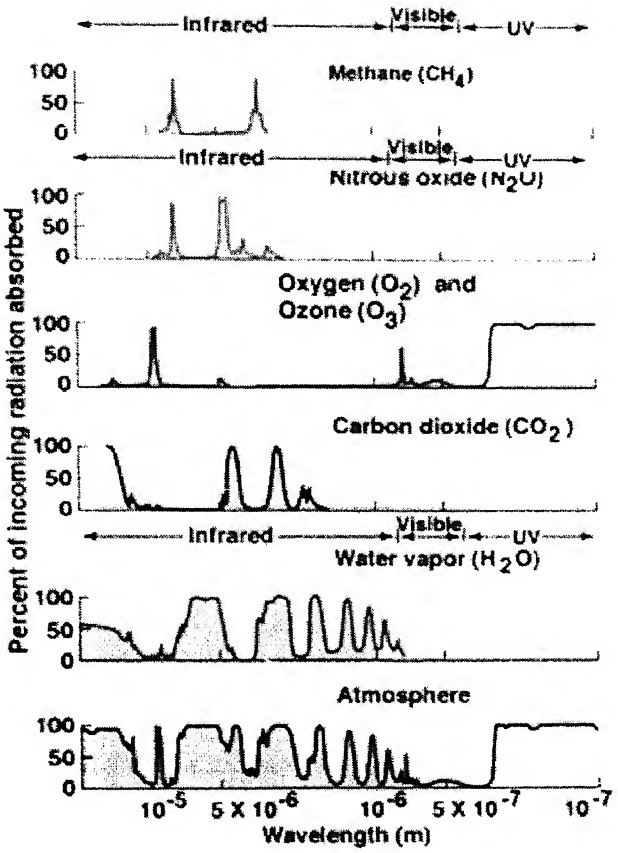

Figure 4.9 Absorption spectra of atmosphere and its constituents[36]

The absorption due to various gases and molecules is almost zero for the visible and the near infrared range. The major absorption that takes place is due to ozone which does not affect the terrestrial wireless links.

So, particle absorption (b_{ap}) is primarily due to elemental carbon (soot).

$$b_{ap} = 10[EC]$$

Again, the quantity in bracket is the mass of elemental carbon in $\mu g/m^3$ and 10 is the extinction efficiencies.

The third important parameter that affects the extinction is Rayleigh scattering. As the particle size of the gases is very small in comparison to wavelength, Rayleigh scattering take place [37]

$$\alpha_{ray} = 9.807 \times 10^{-23} \times \left(\frac{273}{T(h)}\right)\left(\frac{1}{\lambda^{4.0117}}\right)\left(\frac{\Pr(h)}{1013}\right)$$

T= atmospheric temperature [K] depending on height,

Pr= pressure [mbar] depending on height,

λ = laser wavelength [nm].

The total extinction for smoke can be expressed as

$$\beta_{ext} = b_{SO4} + b_{NO3} + b_{Coarse} + b_{ap} + b_{ray} \qquad (4.57)$$

The extinction coefficient of smog is the sum of the extinction coefficient of fog and smoke.

In this chapter, the theory of scattering and radiative transfer is discussed at length. The distributions of rain, fog and smog have been discussed and their effect on the attenuation on of the received optical signal is studied. In the next chapter, the simulation of this theoretical study has been given.

CHAPTER 5
SIMULATION STUDY OF THE OUTDOOR OPTICAL WIRELESS LINKS IN RAIN, FOG AND SMOG

5.1 INTRODUCTION

Atmospheric channel forms a major part of an outdoor link. As discussed in chapter 3, it is one of the major design challenges and affects the link in the form of scattering, absorption and turbulence. In chapter 4, we discussed the various means by which these parameters come into effect, viz. rain, fog, and smoke. In this chapter, the simulation studies on the effect of rain, fog, and smog on the outdoor optical wireless links are done and the results are discussed.

Some assumptions were made while studying the parameters. The particle was assumed to be spherical in nature. The medium was considered as homogeneous, i.e, the refractive index is constant for the entire link length. For the calculations of the various cross sections, Mie-Debye theory has been used as it gives an analysis for scattering and absorption by spherical particles. This theory does rigorous treatment of elastic wave scattering by spherical particles in a surrounding medium.

5.2 MIE THEORY

For the calculation of the Mie efficiency the two important parameters to be chosen are the particle size and the refractive index. The refractive index varies with variations in the wavelength. The value of the refractive index for various wavelengths is taken from reference [38]. Similarly we considered the size of the rain drop to be in the range of 0.1 - 3.6 mm and for fog in the range of 0.01 – 40 μm.

We calculated the extinction efficiency using the equation 4.40 and plotted the same as a function of the drop radius in figure 5.1. We see that as the drop radius increases, the extinction cross-section approaches the value of 2. Moreover, we find that the extinction cross section for higher wavelengths remains substantially smaller than the lower wavelengths for radius less than 1 μm. For example, the extinction cross section of 3.6 μm is less than that of 0.65 μm only when the radius of water sphere is

less than 1 μm. We see that at 10.0 μm the first maximum of the extinction cross section occurs at a radius of about 25 μm.

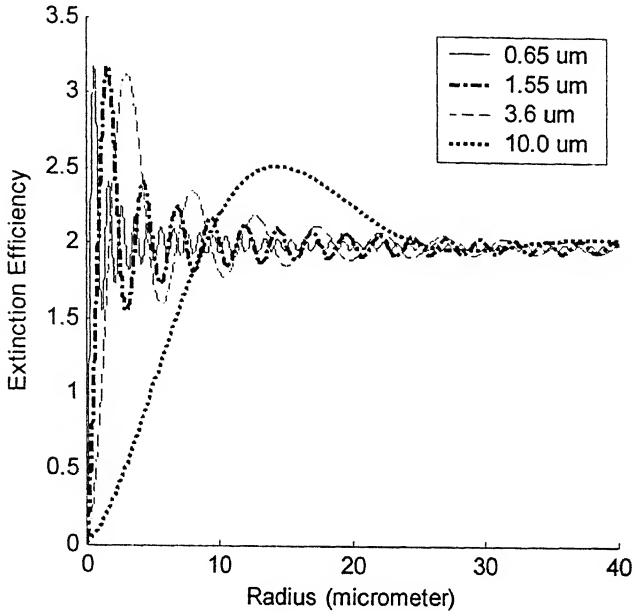

Figure 5.1 Variation of Extinction Cross Section as a function of radius for different wavelengths

The scattering patterns of the electromagnetic waves by spherical particles were studied and it was found that as the particle size increases the scattering decreases. The scattering patterns for fog and rain were calculated using equation 4.39 and are plotted in figure 5.2. From this figure we see that the attenuation due to fog will be much more than that of rain. The reason behind this is that for fog reflection and refraction is dominant, whereas in the case of rain, diffraction plays a major role. As the particle size increases for a fixed wavelength, the diffraction pattern becomes compressed more and more into a narrow but very intense lobe around the forward direction, $\theta = 0$. Hence for such narrow patterns the scattering pattern will be primarily due to diffraction, and for broader beams reflection and refraction will play a major role.

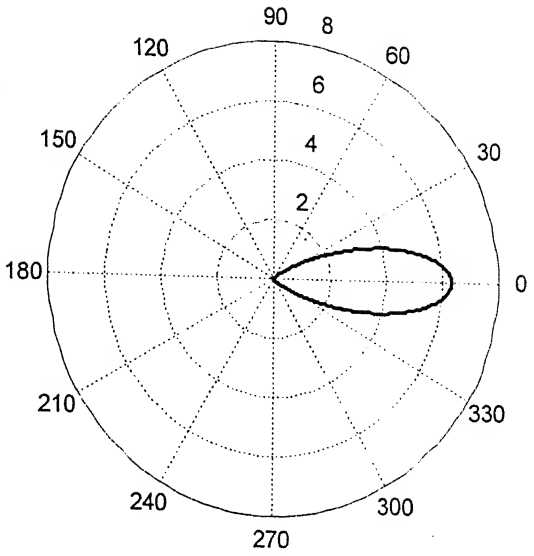

(a)

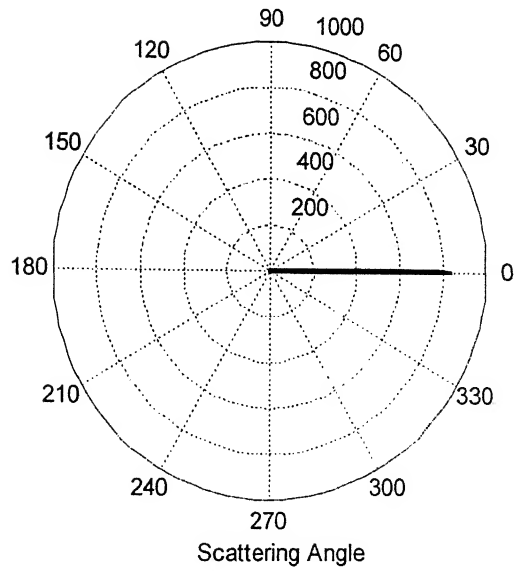

(b)

Figure 5.2 Scattering patterns of electromagnetic wave with spherical particle for wavelength of 670 nm (a) Fog (b) Rain

The scattering and absorption cross sections are calculated using equation 4.41 and 4.42, respectively. The absorption spectrum of the atmosphere for the wavelength

range of 0.5–2 μm is studied and is plotted in figure 5.3. It can be seen from the graph that for absorption coefficient is highly dependent on the wavelength. For few wavelengths, the value of the absorption coefficient is almost zero and hence those wavelengths are suitable for the transmission purposes.

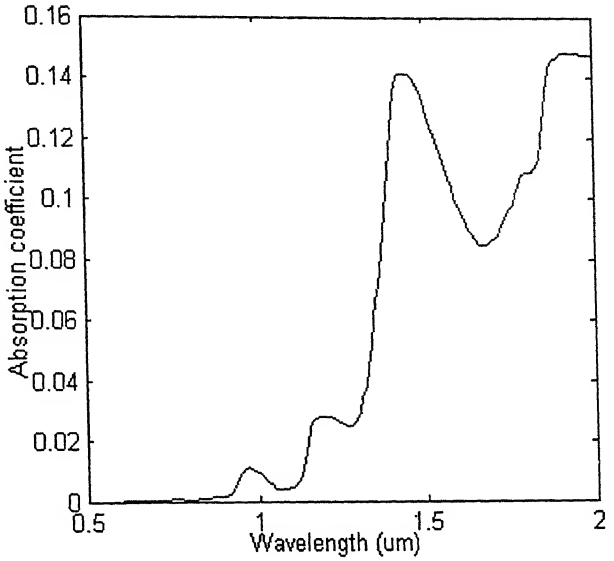

Figure 5.3 Absorption Coefficient as a function of wavelength

The attenuation for the given absorption coefficient can be calculated from equation 4.15. This is plotted in figure 5.4. It is clear from the graph that the attenuation closely follows the absorption coefficient curve and increases as the absorption coefficient increases.

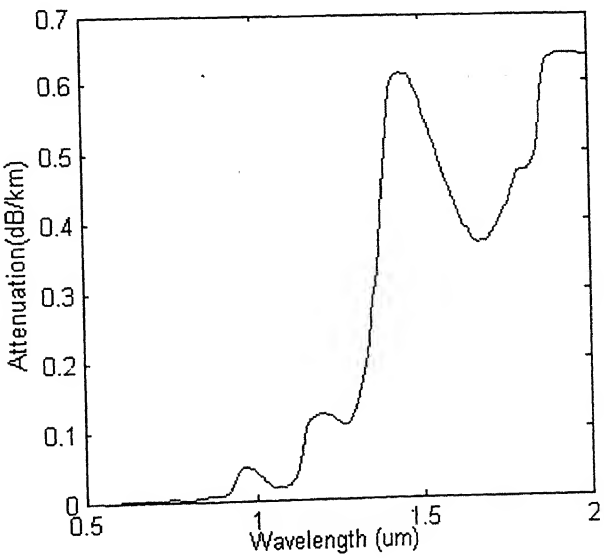

Figure 5.4 Attenuation for a link distance of 1 km as a function of wavelength

The wavelength dependence of the link can be seen from the figure 5.5. We find that the absorption for 670 nm is almost zero and that for 10 μm approaches one as the radius of the drop increases. As the extinction cross section is the sum of the scattering and absorption cross sections, we can conclude that for 670 nm the loss is due to scattering only. However, at 10 μm as the radius of the drop increases, the loss is contributed equally by absorption and scattering.

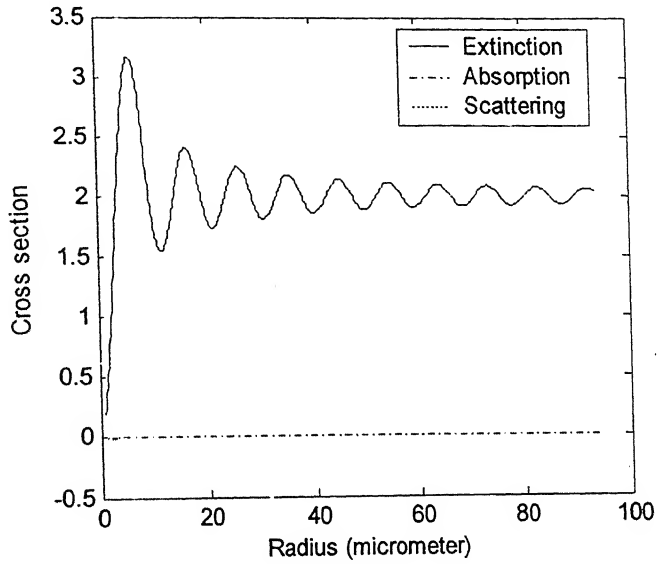

(a)

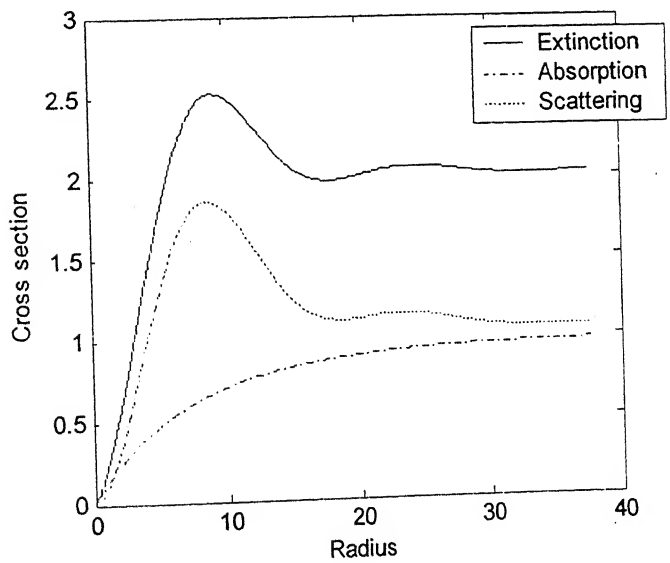

(b)

Figure 5.5 Mie Cross sections for wavelength (a) 670 nm (b) 10 μm

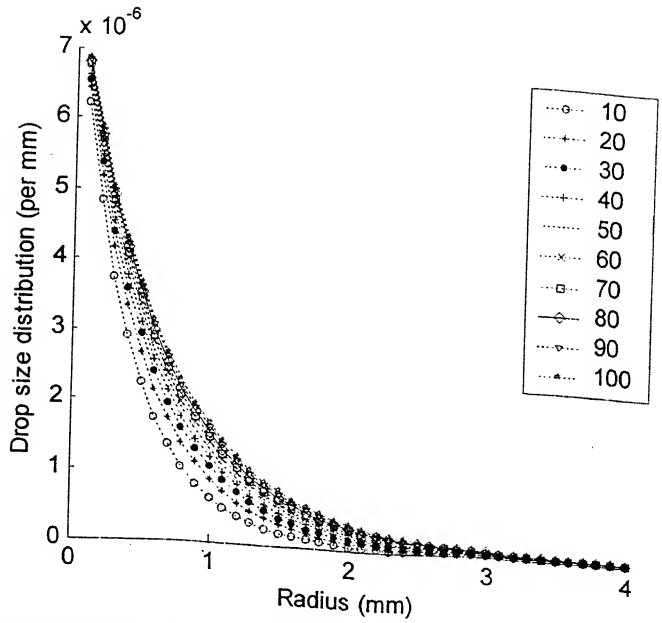

Figure 5.7 Drop size distribution for different rain rates in mm/hr using Marshal and Palmer distribution

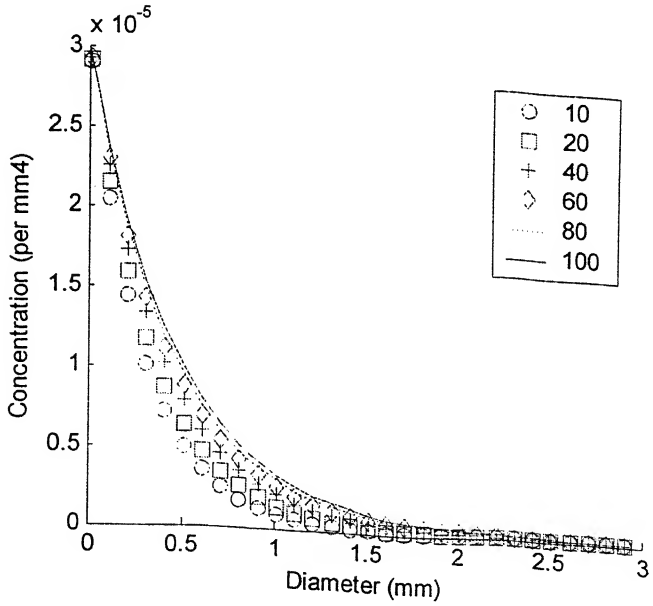

Figure 5.8 Drop size distribution for different rain rates in mm/hr using Drizzle 'JD' distribution

The next distribution studied is the 'Drizzle'-JD distribution. Equation 4.46 is used to calculate the drop size distribution for different rain rates and this in plotted in figure 5.8. This distribution is applicable for very light widespread rain, or drizzle, composed mostly of small drops and is valid for temperate climates. It can be seen from

the graph that the maximum drop size possible for the distribution is only till 1.5 mm. The pattern of the distribution resembles the Marshal and Palmer distribution but the concentration of the drops is very less for a given volume.

The next distribution studied is Weibull distribution for which equation 4.47 is used to calculate the drop size distribution for different rain rates. We show this result in figure 5.9. This distribution is applicable to countries having climate similar to Japan. From the graph, we see that as the rain rate increases the concentration for bigger particle is more than the particles having smaller diameter. Also, as the rain rate increases the diameter of the particle increases.

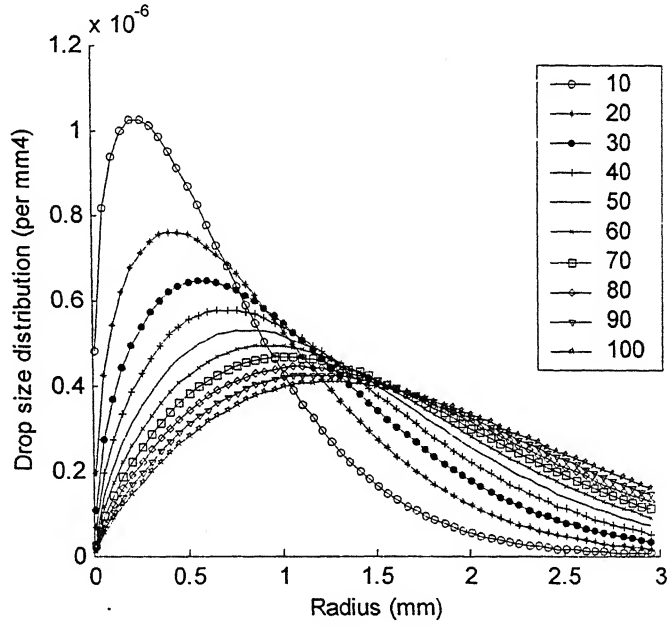

Figure 5.9 Drop size distribution for different rain rates in mm/hr using Weibull distribution

We also studied the gamma distribution and the Log-normal distribution to calculate the drop size distribution for different rain rates. Results for the gamma distribution are plotted using equation 4.48 in figure 5.10. Log-normal distribution results made use of equation 4.49 and are plotted in figure 5.11. This distribution is applicable for countries having climate similar to India. From the graph, we see that as the rain rate increases the concentration of the smaller diameter drop also increases. Also for gamma distribution, as the rain rate increases the median diameter of the particle decreases from 0.5 mm to a very small value.

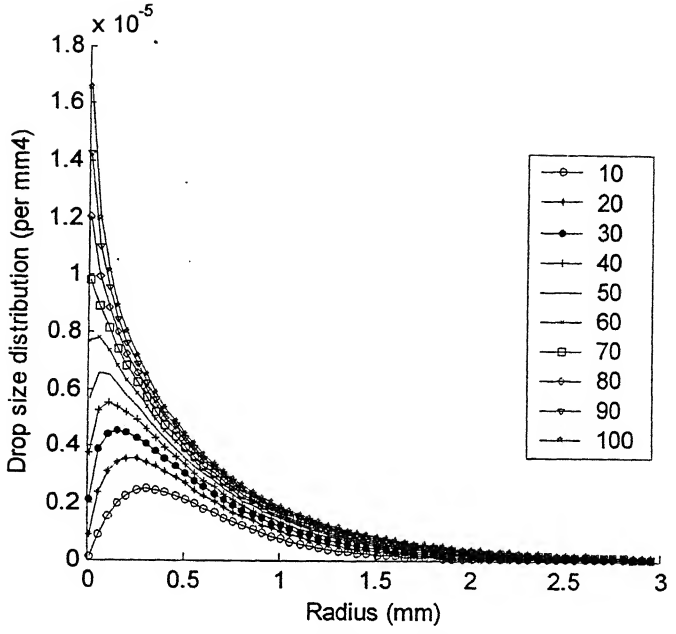

Figure 5.10 Drop size distribution for different rain rates using Gamma distribution

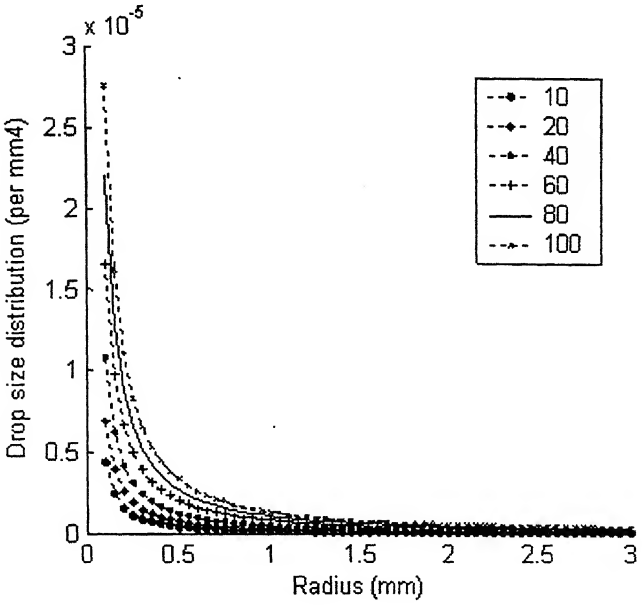

Figure 5.11 Drop size distribution for different rain rates using Log-normal distribution

After studying all the rain drop distributions, we can generalize the distributions on certain points. The contribution of larger rain drops increases with the rainfall rate. Regardless of the rainfall rate, most of the contribution of raindrops comes from drops of about 0.5 mm diameter. This indicates that the contribution of larger drops is small. We see that the mean of raindrop diameters increases with the rainfall rate.

5.3.2 Attenuation Characteristics

Extinction coefficients at different wavelengths as a function of the rain drop diameter are plotted in figure 5.12. It is clear from the figure that the scattering due to rain is geometric scattering and hence is independent of wavelength.

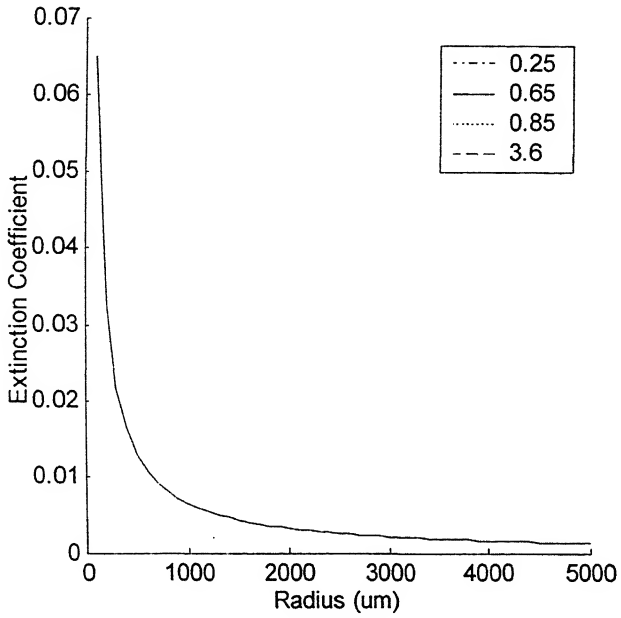

Figure 5.12 Extinction coefficients for different wavelengths as a function of the rain drop diameter

The attenuation coefficient as a function of the rain rate was calculated using equations 4.15 and 4.43 and is plotted in figures 5.13. It is found that the attenuation increases with the increase in the rain rate. We also see that the attenuation is independent of the wavelength employed.

The attenuation for different rain rates is calculated using equation 4.43 for the different drop size distributions. These results are compared in figure 5.14. It can be seen from the above plot that for rain rates less than 20 mm/hr almost all the distributions show the same attenuation. But as the rain rate increases beyond 20 mm/hr, the attenuation calculated for different distributions differs. The lognormal distribution is found to overestimate the value of the attenuation at high rain rates and hence is not suitable for rain rates greater than 50 mm/hr. Gamma distribution which is valid for

Indian sub continent is closely followed by Marshall and Palmer and Weibull Distribution.

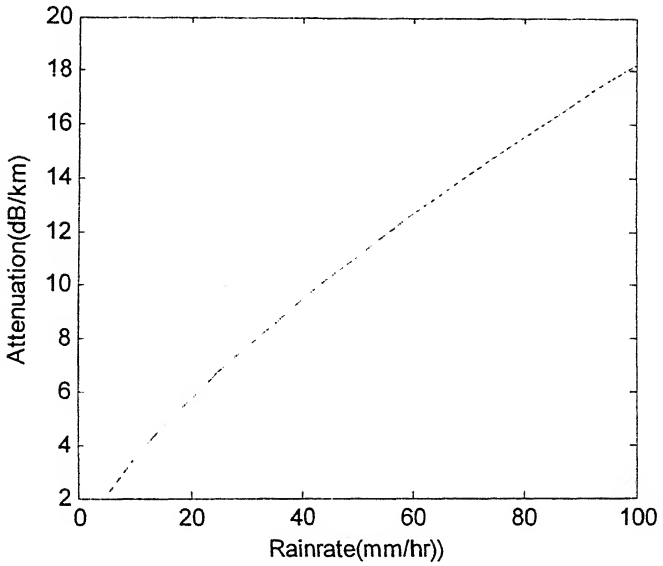

Figure 5.13 Attenuation as a function of rain rate

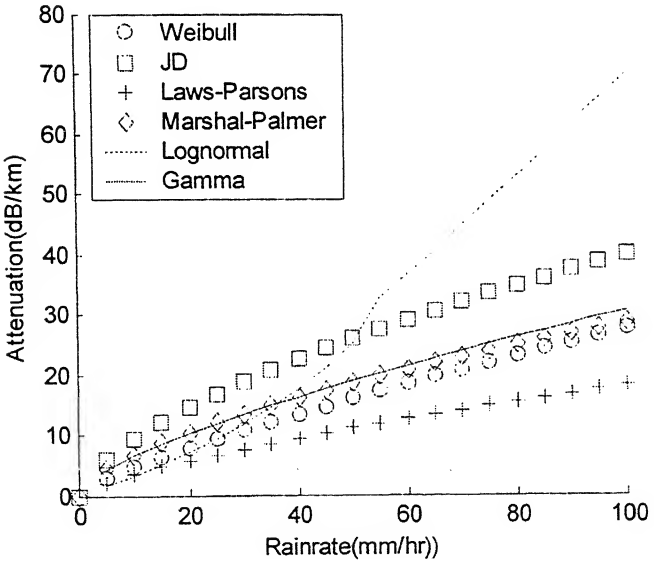

Figure 5.14 Attenuation for different distributions as a function of rain rate

5.3.3 Verification of Simulation Result

We give below the weather parameters from reference [39] for the Huntsville Alabama area on July 04 2001. These data will be applied to the theoretical rainfall model developed to predict visibility.

The Laws and Parsons distribution is employed to calculate the attenuation and the visibility.

Time	Visibility	Precipitation	Events
6:53 PM	5.0 miles / 8.0 kilometers	0.02 in / 0.1 cm	Rain
8:24 PM	3.0 miles / 4.8 kilometers	0.10 in / 0.3 cm	Rain
8:53 PM	8.0 miles / 12.9 kilometers	0.11 in / 0.3 cm	Rain
9:53 PM	10.0 miles / 16.1 kilometers	0.06 in / 0.2 cm	Rain

Table 5.1 Weather parameters for Huntsville Alabama on July 04, 2001 [39]

The first simulation was done using the first set of data, i.e., for visibility of 8.0 km. It is found that the attenuation calculation based on the visibility is greater than the one based on drop size distribution. The value of visibility as found from the calculation is 10.2 km.

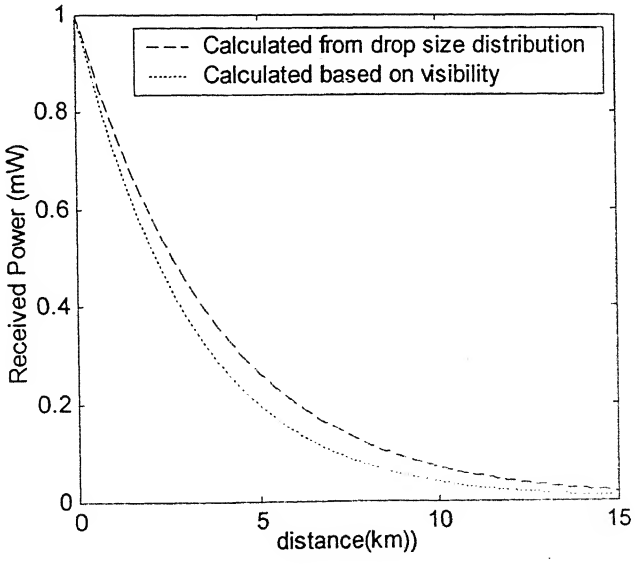

Figure 5.15 Received Power as a function of distance

The second simulation was done using the second set of data, i.e., for visibility of 4.8 km. Here also we find that the attenuation calculation based on the visibility is greater than the one based on drop size distribution. The value of visibility as found from the model is 5.03 km.

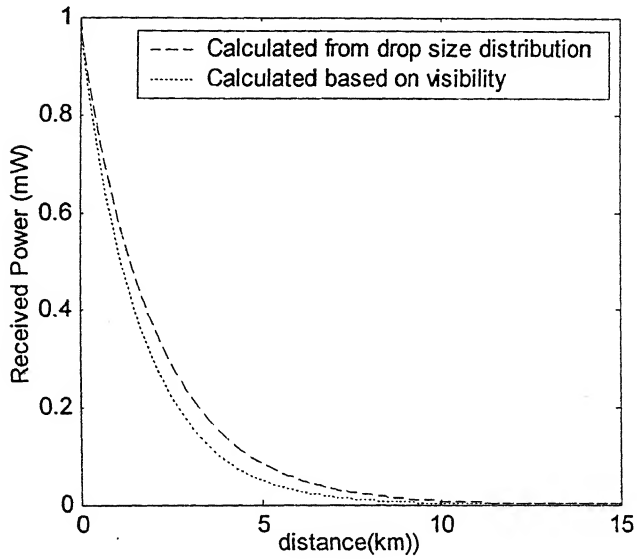

Figure 5.16 Received Power as a function of distance

5.4 FOG

Fog presents one of the major obstacles for outdoor optical communication. In this section, the distribution models of fog and their attenuation characteristics are studied.

5.4.1 Drop Size Distributions

Drop size distribution for fog changes as the visibility condition due to fog changes. The distributions are calculated using Table 4.2. When visibility is less than 100 m, heavy fog distribution is used. Heavy fog contains particles with radius 0.1 to 40 μm.

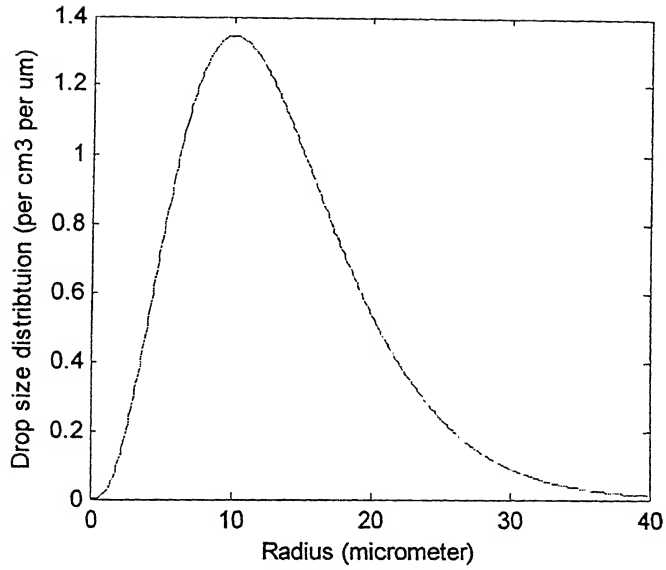

Figure 5.17 Particle size distribution for Heavy fog

When the visibility is less than 500 m, moderate fog distribution is used. Moderate fog contains particles with radius 0.01 to 10 μm.

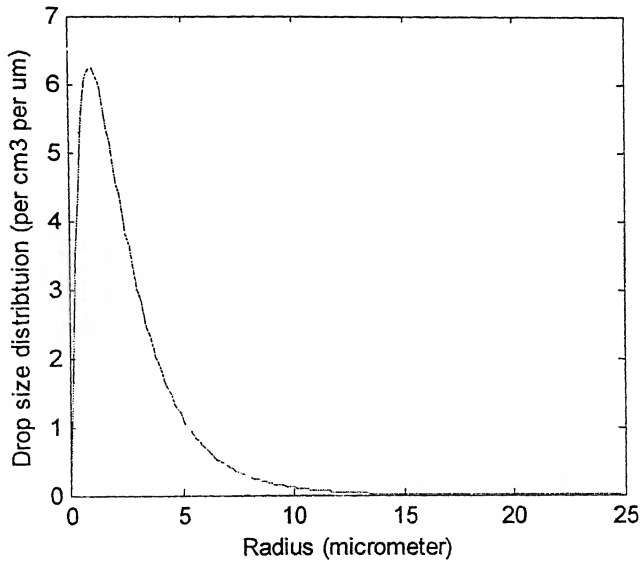

Figure 5.18 Particle size distribution for Moderate fog

When the visibility is less than 2 km, light fog distribution is used. Light fog contains particles of radius 0.01 to 5 μm.

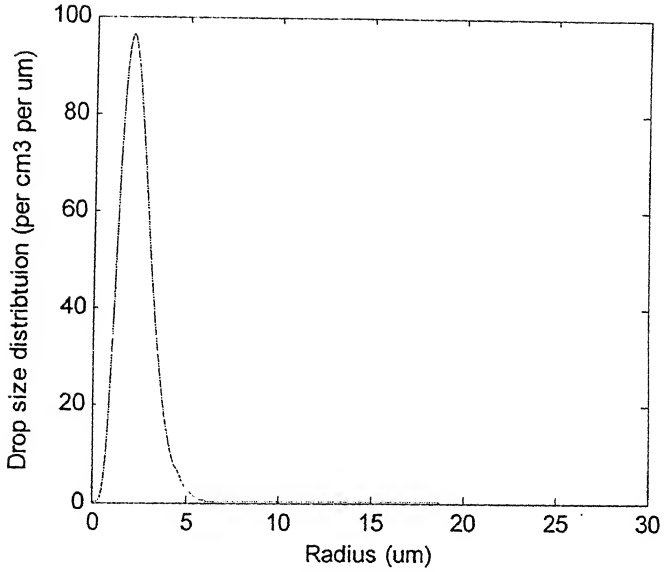

Figure 5.19 Particle size distribution for Light fog

When the visibility is greater than 2 km, haze distribution is used. Haze contains particles with radius 0.01 to 1 μm.

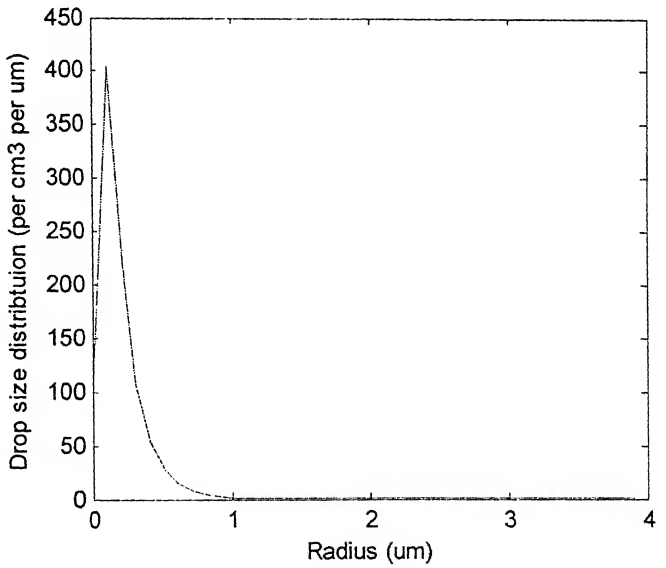

Figure 5.20 Particle size distribution for Haze

From the above graphs, it is clear that as the visibility decreases the radius of the fog sphere as well as the median radius increases.

5.4.2 Attenuation Characteristics

The extinction coefficients for different wavelengths as a function of the particle size are calculated using equation 4.40 and plotted in figure 5.21. We see that as the wavelength increases, the extinction efficiency decreases. Also, the peak of the extinction efficiency shifts from the lower to higher radii as wavelength increases.

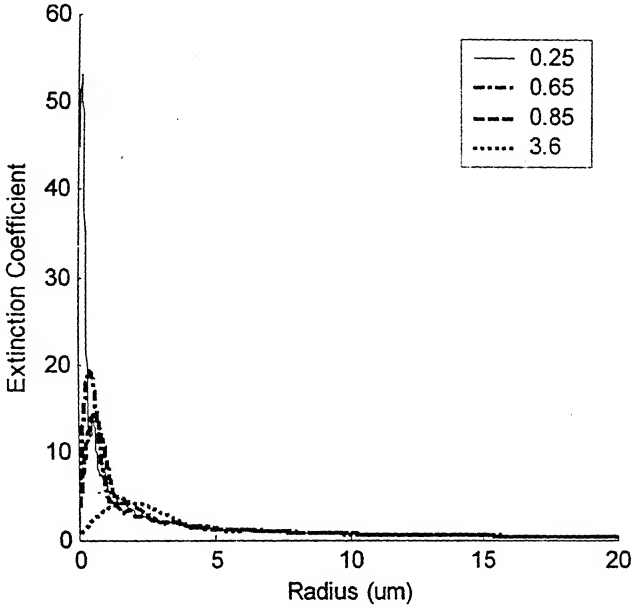

Figure 5.21 Extinction coefficients for different wavelengths as a function of the fog drop diameter

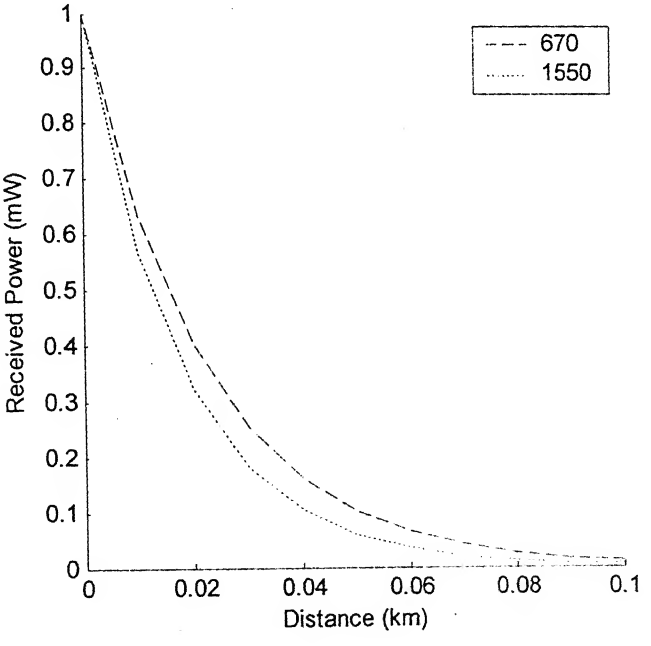

Figure 5.22 Attenuation as a function of distance for heavy fog

Using equation 4.15 we can arrive at the attenuation coefficient for heavy fog at different wavelengths. The attenuation for 670nm is found to be 197.9 dB/km and that for the 1550nm is 247.46 dB/km. We find that in heavy fogs 1550 nm gets attenuated quickly in comparison to 670 nm. The reason for variations in the attenuation in heavy fog with wavelength may be the corresponding variations in the extinction coefficient.

Similarly for moderate fog we can arrive at the attenuation coefficient at different wavelengths using equation 4.15. The attenuation for 670nm is found to be 122.5 dB/km and that for the 1550nm is 125.2 dB/km. The received power for moderate fog with distance is shown in figure 5.33. We find that in moderate fogs, the attenuation for 1550 nm and670 nm is same.

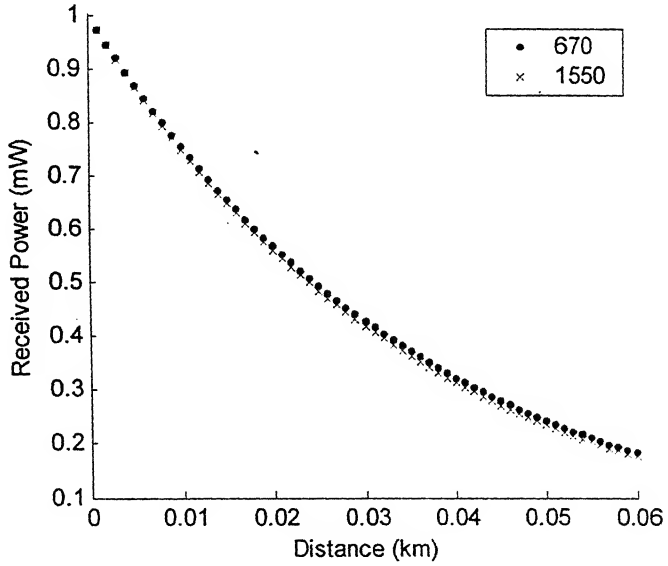

Figure 5.23 Attenuation as a function of distance for moderate fog

A similar approach is used to arrive at the attenuation coefficient for haze. Using equation 4.15 we can calculate the attenuation coefficient for haze at different wavelengths. The attenuation values for 670nm is found to be 0.18 dB/km and that for the 1550nm is 0.06 dB/km The attenuation of the power due to haze with distance is plotted in figure 5.24. The haze distribution shows an increase in the attenuation at 670 nm compared to 1550 nm. The calculated attenuation for the haze distributions are very low and are closer to values expected for clear air.

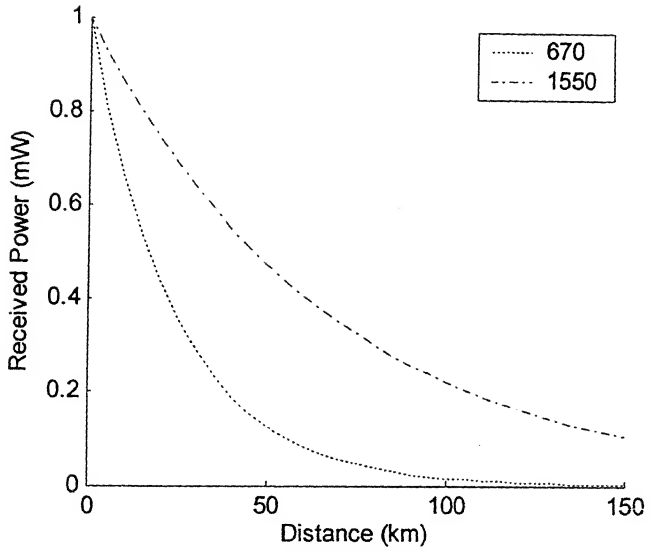

Figure 5.24 Attenuation as a function of distance for haze

5.5 SMOG

Smog is another main parameter which can affect the performance of the OWC link, especially in places with heavy air pollution. Smog comprises of smoke and fog. In this section, the attenuation of the optical power in presence of smog will be discussed. The study will be divided into two parts. First the attenuation characteristics in presence of smoke will be studied and then this will be combined with the characteristics of fog, to get the attenuation due to smog.

5.5.1 Attenuation Characteristics

The extinction coefficient for the given concentration of particular matter and gas in smoke is calculated using the equation 4.57. Various concentration values for the polluted air are taken from the ref [40]. Attenuation over a link distance of 6 km is calculated using equation 4.6.

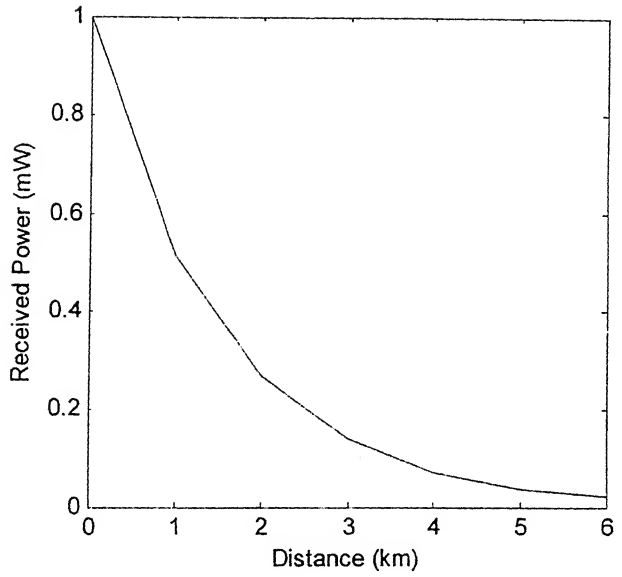

Figure 5.25 Attenuation as a function of distance for smoke

It is seen that even on the days having visibility as high as 200 km in clear air, this figure will drop to a few km with smoke (or polluted air). The value of the extinction coefficient for smoke is 0.6 km^{-1}. Considering dense fog alone the extinction coefficient value is as high as 28. Thus the addition of smoke to this condition does not worsen the situation too much. However, in light fog and haze where the extinction coefficients are typically 4 km^{-1} and 0.05 km^{-1}, respectively, addition of smoke leads to very high losses over the link distance. The attenuation with distance for different types of fog and smog are plotted in figure 5.26 to 5.28.

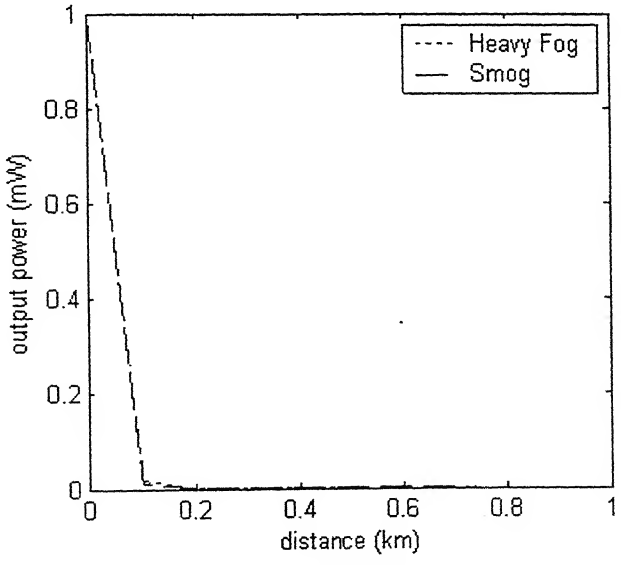

Figure 5.26 Attenuation with distance for smog (heavy fog with smoke) and heavy fog

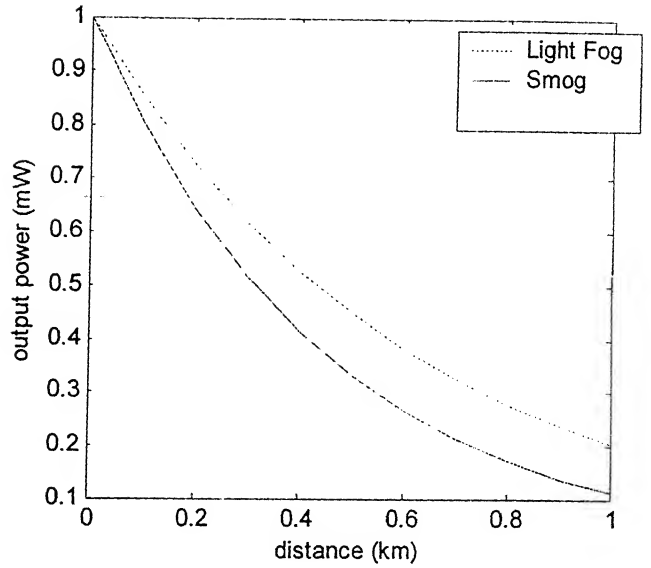

Fig 5.27 Attenuation with distance for smog (light fog and smoke) and light fog

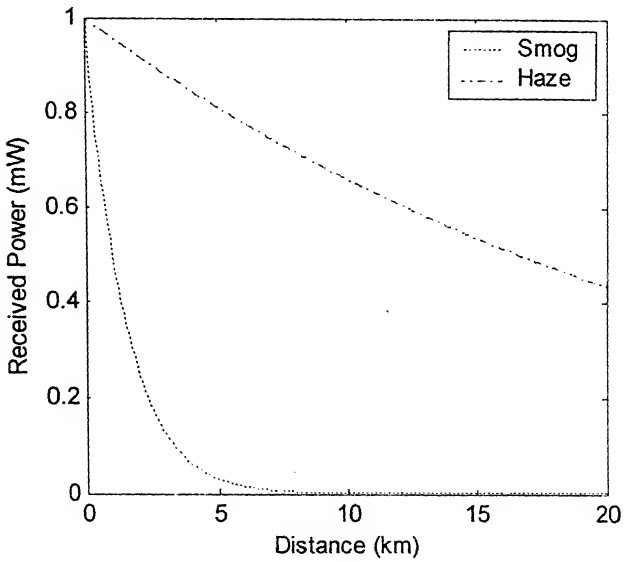

Figure 5.28 Attenuation with distance for smog(haze and smoke) and haze

Table 5.2 summarizes the above results and compares the attenuation of power over the link for various weather conditions. It can be seen from the table that smog affects the link most adversely. If the fog is very dense, then the effect of pollution on the link is not very prominent, but for light fog and haze the pollution affects the link severely. We also see that the effect of rain is less in comparison to fog and smog. The attenuation faced for a rain rate of 100mm/hr is 18 dB/km as compared to an attenuation of 206.06 dB/km faced by the link in heavy fog.

Link Distance	Weather		Attenuation (dB)
500 m	Rain	10 mm/hr	1.74
		50 mm/hr	5.53
		100 mm/hr	9.11
	Fog	Heavy	103.03
		Moderate	19.61
		Light	10.17
	Smog	Heavy	104.99
		Moderate	21.04
		Light	11.61
1000 m	Rain	10 mm/hr	3.48
		50 mm/hr	11.07
		100 mm/hr	18.22
	Fog	Heavy	206.06
		Moderate	39.21
		Light	20.35
	Smog	Heavy	209.98
		Moderate	42.08
		Light	23.22
2000 m	Rain	10 mm/hr	6.97
		50 mm/hr	23.35
		100 mm/hr	40.71
	Fog	Heavy	412.12
		Moderate	78.44
		Light	40.71
	Smog	Heavy	419.97
		Moderate	84.17
		Light	46.44

Table 5.2 Attenuation for different link distances for wavelength = 750 nm and transmission power = 1 mW

5.6 SIMULATION PACKAGE

A simulation package has been designed which can perform all the conditions listed above. It can calculate the attenuation for a given link in various weather conditions. User has to provide some basic information, such as, the transmitter power, the wavelength employed, link distance. Given these conditions, the software will estimate the output power at the receiving end and will also plot various atmospheric effects on the received output power. The GUIs of the simulation package are presented below:

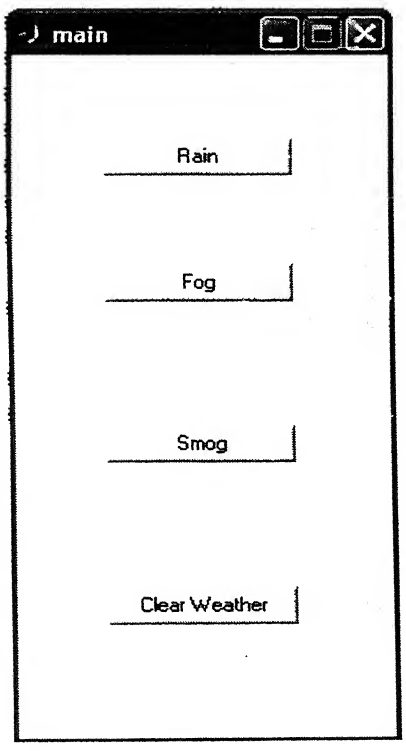

(a)

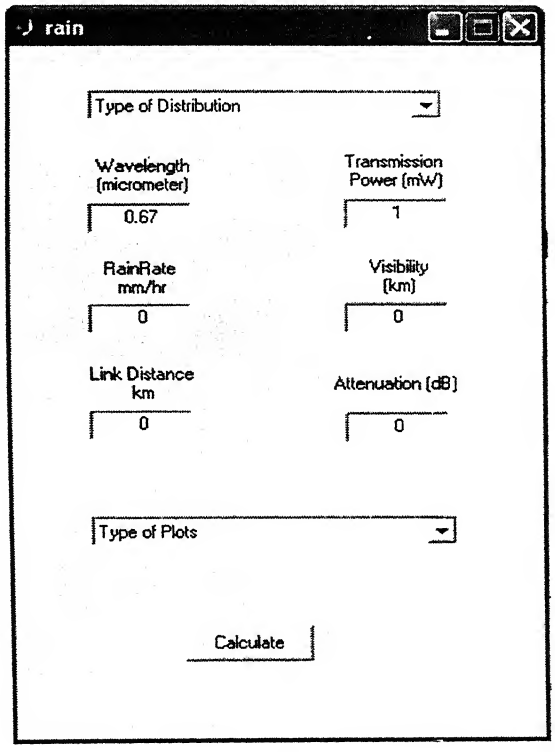

(b)

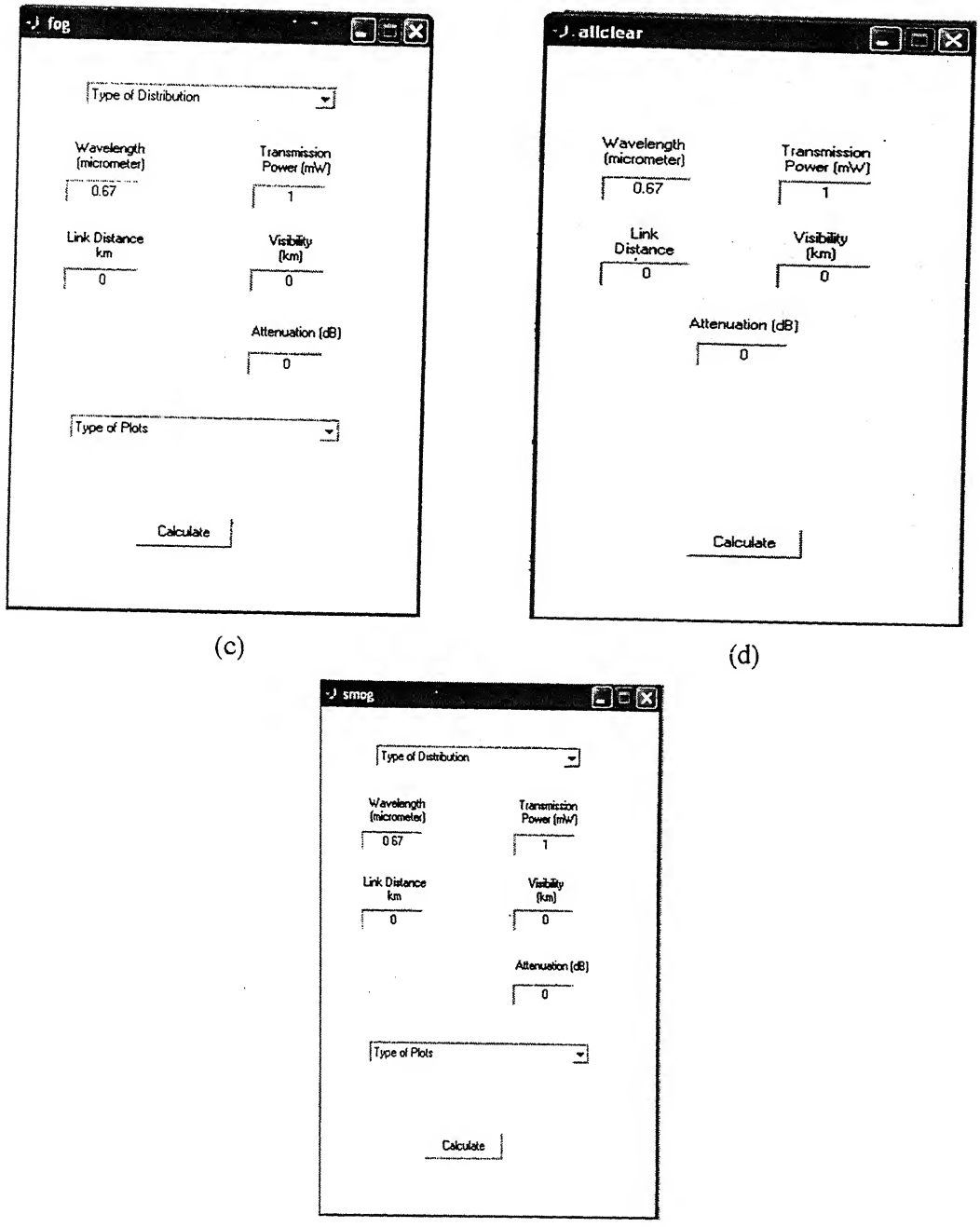

Figure 5.29 GUI of Simulation package

(a) Main Window (b) Rain Calculation Window

(c) Fog Calculation Window (d) Clear Weather calculation Window

(e) Smog Calculation Window

Table 5.3 compares the attenuation over the link under various weather conditions for the wavelengths 785 nm and 1550 nm. These results have been generated using the simulation package.

Wavelength	Weather Conditions			Attenuation (dB)
	Rain	Fog	Smoke	
785 nm	Heavy	-	-	18.22
	Drizzle	-	-	1.09
	-	Heavy	-	207.12
	-	Light	-	17.58
	-	Heavy	✓	209.98
	-	Light	✓	20.02
1550 nm	Heavy	-	-	18.22
	Drizzle	-	-	1.09
	-	Heavy	-	247.56
	-	Light	-	26.94
	-	Heavy	✓	250.42
	-	Light	✓	29.81

Heavy Rain (Rain rate = 100 mm/hr), Drizzle (Rain rate = 2 mm/hr),
Heavy Fog (Visibility = 90 m), Light Fog (Visibility = 1.5 km)

Table 5.3 Attenuation for a link distance of 1 km and transmission power of 1 mW for various weather conditions using the simulation package

CHAPTER 6

CONCLUSIONS AND SUGGESTIONS FOR FURTHER WORK

The aim of the present work was to study the effect of atmospheric conditions like rain, fog and smog on the performance of outdoor optical wireless communication systems. Various weather conditions were studied theoretically and their effects on OWC links were simulated. The main results can be summarized as below:

- Smog affects the link most severely. Attenuation due to fog is more than rain. In case of fog, reflection and refraction are dominant, whereas in the case of rain, diffraction plays a major role.

- The extinction coefficient for fog varies with the size of the drop but for rain it approaches a constant value of 2. For lower wavelengths, the extinction coefficient consists of only scattering whereas at higher wavelengths, both scattering and absorption plays a dominant role in the calculation of extinction coefficient.

- For all the rain drop size distribution models, the contribution of larger rain drops increases with the rainfall rate. Regardless of the rainfall rate, most of the contribution of raindrops comes from drops of about 0.5 mm diameter. This indicates that the contribution of larger drops is small. The mean of raindrop diameters increase with the rainfall rate.

- The attenuation increases almost linearly with the rain rate and is independent of the wavelength employed. The attenuation can be as high as 18 dB/km for a rain rate of 100 mm/hr.

- In heavy fog conditions, attenuation is very high and hence the operational link distance gets reduced to a few meters.

- The 1550 nm wavelength light gets attenuated more quickly than the 670 nm one in case of heavy fog due to the high value of extinction coefficient. But for haze, 670 nm gets attenuated more quickly than 1550 nm.

- In very heavy fog, the effect of smoke is not prominent, but for light fog and haze conditions, smoke in the air leads to very high losses over the link.

- While selecting a wavelength the following points should be considered along with the weather conditions of the place where the link is to be established.

a) Attenuation due to rain is independent of wavelength
b) Attenuation due to heavy fog is high at 1550 nm.
c) Attenuation due to light fog and haze is low for 1550 nm.

6.1 SUGGESTION FOR FURTHER WORK

- This study was basically done for a homogeneous medium. It can be extended to incorporate the effects of random non-homogeneous medium, i.e., turbulence.
- In this thesis, only the attenuation of the link is studied. The effect on bit error rate and the maximum operable data rate can also be studied.
- The results of the thesis may be verified by setting up an outdoor optical wireless link of length, say 1km, between two buildings and measuring the link loss under various weather conditions.
- The rain, fog, and smog drop-size distribution for the city like Kanpur can be studied, which will give an understanding on the various kinds of atmospheric losses faced by an optical link.
- In a country such as India fine dust is a problem during the dry months. The effect of dust may also be studied.

REFERENCES

1. D.Kedar and S.Arnon, "Urban optical wireless communication networks: the main challenges and possible solutions", *IEEE Commun. Mag.* pp. 3-7, 2003.
2. R.M. Gagliardi and Sherman Karp, *Optical Communication.* 2nd ed. A Wiley – Interscience Publication.
3. I.I. Klm *et. al.*, "Wireless optical transmission of fast Ethernet, FDDI, ATM, and ESCON protocol data using the TerraLink laser communication system", *Opt. Eng.*, vol. 37, pp. 3143-3155, 1998.
4. W.R.Leeb, "Degradation of signal to noise ratio in optical free space data links due to background illumination" *Appl. Opt.*, vol. 28, pp. 3443-3449, 1989.
5. F.Capasso *et.al.* , "Quantam cascade lasers: ultrahigh-speed operation, optical wireless communication, narrow line width and far infrared emission", *IEEE J. Quantam Electron.* , vol. 38, pp. 531-532, 2002.
6. E.Brookner, "Atmospheric propagation and communication channel model for laser wavelengths" , *IEEE Trans. Commun. Technol.*, vol. 18, pp. 396-416, 1970.
7. J.I.Davis, "Consideration of atmospheric turbulence in laser systems design", *Appl. Opt.* , vol. 5, pp. 139-145, 1966.
8. B.R.Strickland, "Effects of fog on the bit error rate of a free space laser communication systems", *Appl. Opt.*, vol. 38, no. 3, pp. 424-431, January 1999.
9. Timothy L. Grotzinger, "Atmospheric effects on FSO systems", *www.laserwireless.net, 2005.*
10. I.I.Kim *et. al.*, "Comparison of laser beam propagation at 785 nm and 1550 nm in fog and haze for optical wireless communications", *Proc. SPIE Optical Wireless Communication III,* vol.. 4214, pp. 26-47, 2000.
11. A.Acampora, "Uninet: A hybrid approach for universal broadband access using small radio cellsinter-connected byfree space optical links", *IEEE J. Select. Areas Commun.*, vol.16, pp. 973-987, 1998.

12. M.Achour, "Simulating atmospheric free-space optical propagation part i: rainfall attenuations", *Proc. SPIE Optical Wireless Communication V*, vol. 4873, pp 1-12, 2002.
13. M.Achour, "Simulating atmospheric free-space optical propagation part ii: haze, fog and low clouds attenuations", *Proc. SPIE Optical Wireless Communication V,* vol. 4635, pp 21-31, 2002.
14. Manoj Satle, "*Studies on the performance of outdoor optical wireless systems under atmospheric conditions*" M.Tech thesis IIT Kanpur 2003.
15. http://www.dominionlaser.com
16. http://www.laserwireless.net
17. http://www.lightpointe.com
18. http://www.cablefreesolutions.co.uk
19. http://www.plaintree.com
20. http://www.opticalaccess.com
21. hhtp://www.fsona.com
22. http://www.laserbit.com
23. David A. Rockwell *et. al.*, "Wavelength selection for optical wireless communication systems", *Optical Wireless communications IV, Proc. Of SPIE,* vol. 4530, pp. 27-35, 2001
24. Christian E. Junge, *Air chemistry and radioactivity,* Academic Press, 1963.
25. H.C.V. De Hulst, *Light scattering by small particles*, JohnWiley & Sons Inc., New York, 1957.
26. R.M.Lerner, "The optical scatter channel", *Proc. IEEE*, vol. 58, pp. 1547-1563, 1970
27. W.E. Knowles Middleton, *Vision through atmosphere*, University of Toronto Press, 1969
28. M.Kerker, *The scattering of light and other electromagnetic radiation*, Academic Press, 1963.
29. R.S.Olsen *et. al.*, "The aR^b relation in the calculation of rain attenuation", *IEEE*

30. D.A. de Wolf, "On the laws-parsons distribution of raindrop sizes", *Radio Sc.*, vol. 36, 4, pp. 639-642, 2001.
31. H. Jiang *et. al,* "Weibull raindrop-size distribution and its application to rain attenuation", *IEE Proc. Microwave Ant. Prop.*, vol. 144, , pp. 197-200, 1997.
32. Ajayi *et. al.,* "Modeling of a tropical raindrop size distribution for microwave and millimeter wave applications", *Radio Sc.*, vol. 20 pp. 193-202, 1985.
33. A. Maitra, "Three Parameter raindrop size distribution modeling at tropical location", *Electron. Lett.*, vol. 36, pp. 906-907, 2000.
34. D. Deirmendjian, "Scattering and polarization properties of water, clouds and hazes in the visible and infrared", *Appl. Opt.* , vol. 3, p.p 187-196, 1964.
35. T.S.Chu *et. al,* "Effects of Precipitation on Propagation at 0.63, 3.5 and 10.6 Microns", *Bell Syst. Technol. J.*, pp. 723-759, 1968.
36. http://www2.nature.nps.gov/air/Permits/flag/app2a.html
37. L.Elterman, "UV, Visible and IR attenuation for altitudes to 50 km, 1968", *Environ. Research Papers*, no 285, 1968.
38. D. J. Segelstein, "The complex refractive index of water", Mtech Thesis, University of Missouri, Kansas City, 1981
39. http://www.wunderground.com/history/airport/KRMG/2001/6/29/Dailyhistory.html
40. C.Venkatarman *et.al,* "Aerosol size and chemical characteristics at Mumbai, India, during the INDOEX-IFP (1999)", *Atmos. Environ.* , vol. 36, pp. 1979-1991, 2002.